

Máster en Física Avanzada

Especialidad en Física Nuclear y de Partículas



Trabajo Fin de Máster

Faraway algorithm to reconstruct and trigger vertices from Long-Living Particles at LHCb

Volodymyr Svintozelskyi

Tutor: Prof. María Aránzazu de Oyanguren Campos

Curso académico 2024/25

Abstract

The Standard Model and many new physics scenarios predict the existence of long-lived particles (LLPs), with lifetimes larger than 100 ps. However, the reconstruction and selection of these particles are very challenging at the Large Hadron Collider (LHC) due to their significantly displaced decay point. Because of the recently upgraded LHCb detector and the new GPU-based first High-Level Trigger (HLT1) it became possible to develop brand-new algorithms for fast track reconstruction without the usage of the hits from the first two trackers (VERtex LOcator and Upstream Tracker). The **Faraway** track reconstruction algorithm, developed in the framework of this master thesis work, uses only hits in the new large Scintillating Fibre Tracker (SciFi) to reconstruct secondary vertices formed by LLPs. The algorithm utilises a new procedure for fast extrapolation of the tracks through the LHCb magnetic field. In addition, it uses a fully connected single-layer Neural Network (NN) for fake vertex rejection. The algorithm is validated using mass distributions of K_S^0 and Λ hadrons from the real data collected during the 2024 LHCb operation. It is expected that the **Faraway** reconstruction algorithm will extend the LHCb physics potential during future data-taking periods.

Contents

1	Introduction.	5
2	Long-living Particles (LLPs)	6
3	Long-Lived Particles Beyond the Standard Model	7
3.1	Hidden Sector particles	8
3.2	Heavy Neutral Leptons (HNLs)	8
3.3	Axion-Like Particles (ALPs)	9
4	Experimental status	9
5	Large Hadron Collider (LHC)	10
6	The LHCb experiment	12
6.1	VERTex LOcator (VELO)	13
6.2	Upstream Tracker (UT)	13
6.3	Scintillating Fibre Tracker (SciFi)	15
6.4	Magnet	16
7	Track description and types at LHCb	16
7.1	Track description model	17
8	The LHCb trigger system	18
8.1	High Level Trigger 1 (HLT1)	19
8.2	High Level Trigger 2 (HLT2)	19
9	Track reconstruction algorithms at HLT1	19
9.1	<i>VELO</i> track reconstruction	20
9.2	<i>SciFi</i> track reconstruction	20
9.2.1	Partial reconstruction in xz plane with Seeding_XZ	20
9.2.2	Charge-momentum estimation and tolerance windows	21
9.2.3	Adding uv information and confirmation	22
9.3	<i>Long</i> track reconstruction	24
9.4	<i>Downstream</i> track reconstruction	24
10	Studies of sensitivity to BSM particles	25
11	Faraway reconstruction algorithm	26
11.1	<i>SciFi</i> track segments and momentum resolution	27
11.2	Extrapolation model	28

11.3 Trajectory function studies using standard LHCb MC samples	28
11.4 Trajectory function studies using a dedicated simulation setup	30
12 Vertex reconstruction algorithm	32
13 Fake vertex killer	32
14 Selection of particle candidates	34
15 Algorithm implementation	34
16 Algorithms performance	37
17 Prospects	37
17.1 Improvement of the trajectory function using MVA	37
17.2 Usage of reconstruction information from other sub-detectors	40
17.3 The potential of <i>faraway</i> track reconstruction	41
18 Conclusions.	42
References	43

Acknowledgments

I want to take the opportunity to mention and express my deepest gratitude to everyone who made this work possible and supported me throughout my journey.

Most importantly, my sincere appreciation to my supervisor, Prof. María Aránzazu de Oyanguren Campos, for her endless guidance, immense support and wisdom that became crucial for my academic growth. Thank you so much for your presence during all the important periods in the past two years, including but not limited to the preparation of my talks, reports and now the current thesis, my journey to CERN and Hamburg. And even during the darkest times of Ukrainian electricity blackouts, border crossing restrictions, and eventual relocation, you still were there and supported me and my work.

I also want to thank the members of the IFIC-LHCb group for their insights, ideas, stimulating discussions and help throughout my work: Brij, Fernando, Izaac, and Valerii. I especially want to express my gratitude to Jiahui, as without you I wouldn't managed to get to the bottom of not only the LHCb software stack but also the existing algorithms used for reconstruction.

In addition, I would like to mention Maksym Ovchynnikov for your expertise and availability even for the last-minute questions, that arise during my work.

Last but not least, I want to thank my parents for all the support you gave me, the inspiration you provided, and for believing in me from the very beginning.

1 Introduction.

The Standard Model (SM) of particle physics is the most successful fundamental physics theory up to now. Its purpose is to describe the basic properties of matter, including the interactions among particles. The SM describes three of the four fundamental forces in nature: the electromagnetic force, the strong force, and the weak force. It does not include gravity, which is described by the theory of general relativity. According to the SM, matter is made up of particles with spin 1/2: quarks, and leptons. Both of them are called fermions. Quarks are the building blocks of protons and neutrons, which make up atomic nuclei, while leptons include particles such as electrons and neutrinos (Fig. 1).

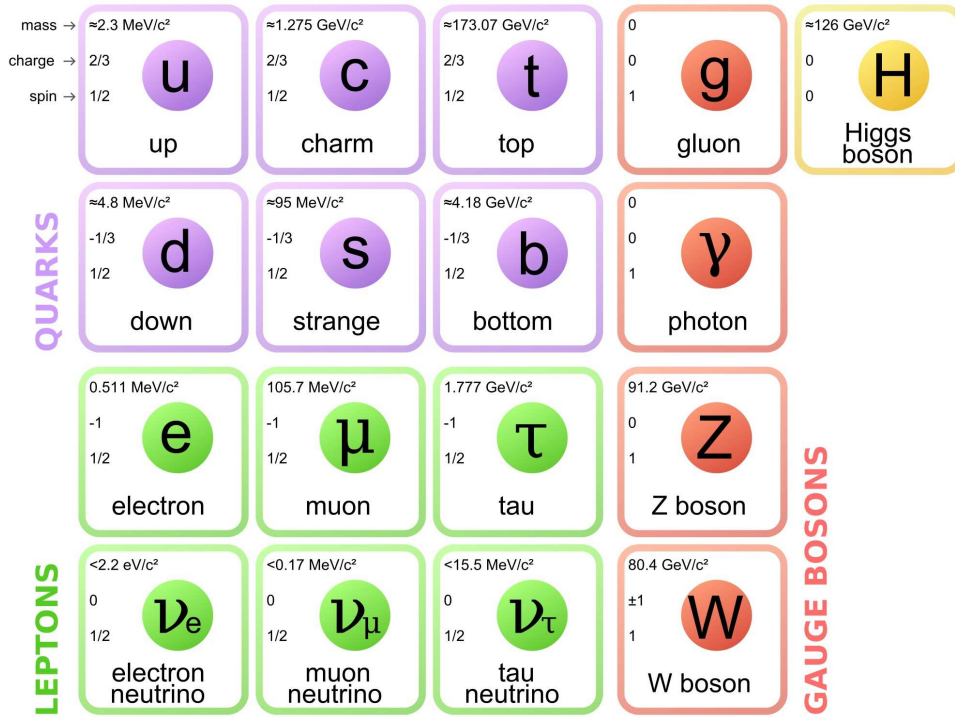


Figure 1: Particle content of the Standard Model. [1]

The interaction between particles is described as an exchange of other particles with spin 1, called bosons. For example, the electromagnetic force is mediated by the photon while the weak force is mediated by the W^\pm and Z bosons. Together, these two forces are called electroweak (EW) force, as they are joined at the fundamental level. On another hand, the strong force, which describes why the quarks are tied together inside protons and neutrons (hadrons), is mediated by the gluon vector boson. The theory of quark-gluon interactions is called Quantum Chromodynamics (QCD).

The Higgs boson, the latest of the discovered bosons of the SM, describes the fundamental mechanism of particle mass [2, 3]. Experiments at the Large Hadron Collider (LHC) at CERN (European Organisation for Nuclear Research) verified the fact that at present the Higgs boson properties match with the SM predictions.

The schematic view of the SM content together with basic particle properties are shown in Fig. 1. The fermions are divided into three generations, each consisting of two quarks with different charges and two lepton types. In addition, mediator spin-1 bosons and the Higgs boson are shown in this table. Every particle has a corresponding antiparticle, with the same mass but opposite quantum numbers. Particles with vanishing quantum numbers, such as the Z or γ bosons, are their own antiparticles.

Quarks can be combined together to form various composite particles. Mesons are made of a quark and an anti-quark pair, while baryons consist of three quarks. From the theoretical point of view, the SM is described by a relativistic Quantum Field Theory (QFT) [4]. Within this formulation, different types of quantum fields fill the space-time continuum. The excitations of such fields are the elementary particles, while the interactions between the fields correspond to the fundamental forces explained above (electromagnetic, strong and weak). Mathematically, those interactions are described by the Lagrangian

$$\mathcal{L}_{SM} = \mathcal{L}_{EW} + \mathcal{L}_{QCD} + \mathcal{L}_{Higgs} + \mathcal{L}_{Yukawa}, \quad (1.1)$$

where the terms correspond to, in order, electroweak (EW) and strong (QCD) fundamental forces, interactions between the Higgs and other massive gauge bosons (Higgs), and Yukawa couplings, that describe the interactions between the Higgs and the fermions. The interactions with the Higgs boson via the spontaneous symmetry breaking mechanism [5, 6] is what gives mass to the fermions and to the Z and W^\pm bosons.

Despite the great success of the SM, there are a number of physics phenomena, that still lack theoretical explanations. For example, missing dark matter and dark energy are not explained by SM. In addition, the theory is not consistent with the theory of general relativity, which describes gravity. The reason is that the graviton, the expected mediator particle, has not been observed. The matter-antimatter asymmetry in our Universe remains a mystery that cannot be explained by the SM.

The problems of SM motivate physicists to develop and test new theories, that will provide a better understanding of nature and, maybe, can unify all known forces. Many of the proposed beyond the SM (BSM) involve the so-called "long-lived particles" (LLP), which will be explained in the next section.

2 Long-living Particles (LLPs)

The particle lifetime τ represents the average time an unstable particle exists before it eventually decays. The lifetime is connected to the decay width Γ via inverse proportion $\tau = \frac{1}{\Gamma}$, the quantity that represents the probability of a particle decaying into a specific set of final-state particles per unit of time. The total decay width may be calculated as a sum of all the partial decay widths as $\Gamma = \Sigma \Gamma_i$, where i denotes one particular

decay channel. The decay width depends on the properties of particles participating in the interaction such as mass, type, and strength of the interaction, together with the available phase space. The probability for a particle to decay within a given time interval can be calculated as $P(t) = 1 - e^{-\Gamma t}$. In general, stronger interactions, such as strong nuclear force or electromagnetic force, are associated with short lifetimes.

The vast majority of the particles within the SM have a very short lifetime. The range varies from 10^{-25} s to 10^{35} years. Some of them are considered stable, such as the electron or the proton. A plot of lifetime vs particle mass within the Standard Model is shown in Fig. 2, [7, 8]. Given this wide range, the term "long-lived particle" is ambiguous, and

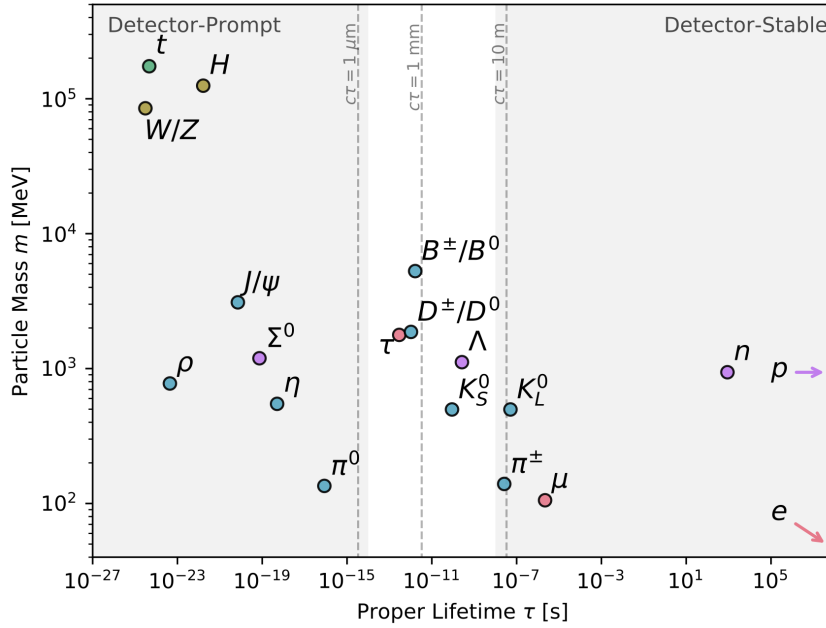


Figure 2: Some of SM particles on the lifetime-mass plane. The plot is divided into three regions: short lifetime (labeled as prompt particles, $c\tau < 1 \mu\text{m}$), lifetime large enough to create displaced vertices ($1 \mu\text{m} < c\tau < 10 \text{ m}$), and "stable" particles from detector's point of view ($c\tau > 10 \text{ m}$)[8].

it usually depends on the experimental framework one is working on. In proton-proton colliders, and in the context of this work, long-lived particles refer to those with lifetimes starting from 100 ps and beyond, which in the SM refers mainly to the strange hadrons K_S^0 and Λ . In many BSM theories, small couplings between the LLP and lighter states also may lead to larger particle lifetimes. Some examples are described in the following section. Within the context of the current work, the geometrical acceptance of the LHCb detector will be crucial to define the sensitivity region to different LLP lifetime ranges.

3 Long-Lived Particles Beyond the Standard Model

Particles with long lifetimes are predicted by many BSM theories. This is, in particular, motivated by the fact that they typically are feebly interacting particles, and therefore very

challenging to be detected by experiments. In addition, LLPs can help in understanding dark matter, and are very relevant in cosmology, as they can be related to leptogenesis and baryogenesis processes in the early Universe [9]. In general, for a LLP with mass m , decaying in a process involving a heavy off-shell particle with mass M , one can express its decay width as

$$\Gamma \sim \frac{\epsilon^2}{(8\pi)^{a-1}} \frac{m^n}{M^{n-1}}, \quad (3.1)$$

where ϵ is a potentially small coupling constant, n is a positive integer that depends on theoretical framework, and a indicates a number of final state particles. The following subsections present a short review of some examples of BSM theories that predict the existence of LLPs.

3.1 Hidden Sector particles

The Hidden Sector models predict new particles, that either weakly interact with SM particles or do not interact at all [10]. Because of that, such particles are very difficult to detect, however they should be accessible with current experimental energies. The Dark Photon (A') and a new Higgs boson (H') are some of the candidates to couple to the new particles. As these particles are hardly visible by experiments, they are good candidates to dark matter. An example Feynman diagram with a heavy scalar (Φ or a Higgs) decaying into long-lived scalars S is shown in Fig. 3.

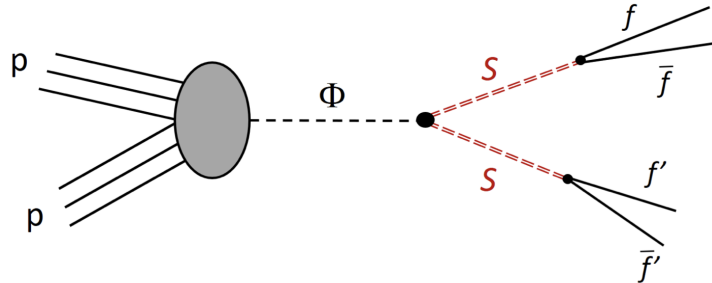


Figure 3: A Feynman diagram showing an example interaction mediated by dark scalars in the Hidden Sector. The final state contains several fermions (f).

3.2 Heavy Neutral Leptons (HNLs)

The SM predicts neutrino to be mass-less, however from experimental results, it is clear that they should have a finite non-zero mass. This caused the development of theories that include new heavy right-handed neutrinos with masses larger than the eV scale, the Heavy Neutral Leptons (HNLs) [11]. Such particles enter in the Yukawa couplings with the lepton doublet and the Higgs field and are nearly sterile, or almost not interacting and therefore being very difficult to detect.

HNLs would help to understand why the SM neutrinos have smaller masses as compared to other fermions, and why the mixing between leptons (described by the PMNS mixing matrix) presents a different structure as compared to the quarks one (described by the CKM mixing matrix). In addition, the existence of HNLs could explain the baryon asymmetry of the early Universe, with the CP violation increase due to the neutrino oscillations. Also, if there are enough HNLs and they are heavy enough, it may constitute a dark matter candidate. An example diagram with HNL interacting with SM particles is shown on Fig. 4.

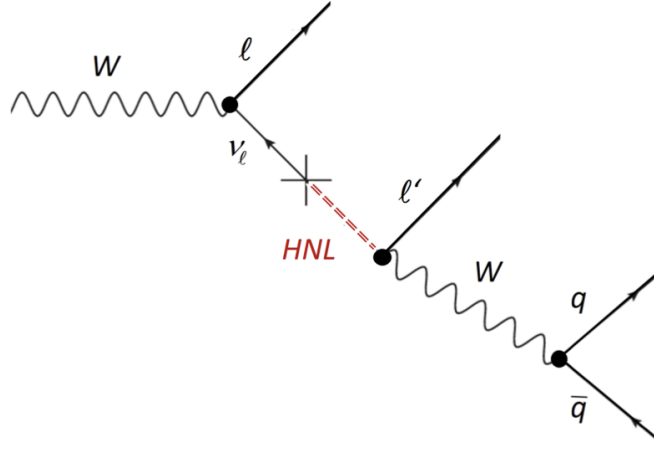


Figure 4: A Feynman diagram showing an example of HNL production via mixing with a SM ν from W boson decay.

3.3 Axion-Like Particles (ALPs)

Several extensions of the SM, such as String theory, predict light, neutral, pseudo-scalar bosons that are expected to interact primarily with two photons. They are called Axion-Like particles (ALPs). They are a generalisation of the axion, the pseudo-Goldstone boson which is related to the global Peccei-Quinn symmetry $U(1)_{PQ}$, proposed as a natural solution to the strong CP problem [12], in attempt to understand why the neutron electric dipole moment (EDM) is small. ALPs are predicted to be very light and interact very weakly, leading to long lifetimes. In addition, they could be a component of dark matter. An example process, mediated by an ALP, is shown in Fig. 5.

4 Experimental status

The LHCb collaboration performed several searches with the data collected during 2011 to 2012 (Run 1) and 2015-2018 (Run 2) of the LHC. Analyses included several experimental signatures such as:

- events with a lepton from a high-multiplicity displaced vertex [13],

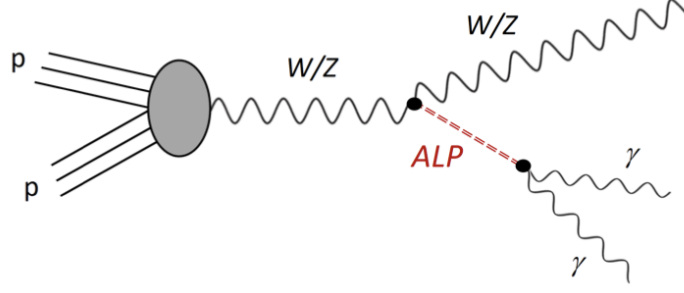


Figure 5: A Feynman diagram showing an example interaction mediated by an ALP particle.

- events with two displaced high-multiplicity vertices [14, 15],
- decays of B mesons (mediated by a Majorana neutrino) to a final state with two same-sign leptons associated to different vertices [16, 17],
- B meson decays to a final state with two opposite-sign leptons forming a displaced vertex [18, 19],
- prompt tracks (charged massive stable particles) extending to the muon stations with velocity lying below the threshold for producing Cherenkov light in the RICH detector [20],
- prompt muons which form a high-quality displaced vertex [21].

The biggest general-purpose experiments (ATLAS and CMS) also performed an extensive LLP search using several signatures: detached muons, photons not pointing to the primary vertices, displaced di-electromagnetic vertices ($H \rightarrow \gamma\gamma$ or $Z \rightarrow e^+e^-$), trackless and delayed jets, and multi-charged particles, are examples of them.

However, until now the majority of the new physics searches were based on the idea of prompt decays wherein particles decay close to the Interaction Point (IP) and decay products traverse through the rest of the detector layers. In contrast, the newly proposed experiments aim to extend the detector sensitivity region by being able to search for new particles with longer lifetimes than before. A comprehensive review of the current status and future proposals of LLP searches across the experiments outlines the importance of LLPs and can be found in [22].

The current work is focused on the upgrade of the present LHCb experiment to detect BSM particles with lifetimes beyond 100 ps.

5 Large Hadron Collider (LHC)

The LHC is located about 100 m depth at the CERN site near Geneva. It is the largest and most powerful particle accelerator in the world, with 27-kilometer circumference.

LHC has been operating since 2010 in three runs: Run 1 (2011-2012) at 7 and 8 TeV center-of-mass energy (\sqrt{s}), Run 2 (2015-2018) at 13 TeV, and Run 3, which started in spring 2022 at $\sqrt{s} = 13.6$ TeV. The LHC beam contains up to roughly 2800 bunches of protons, each having around $1.15 \cdot 10^{11}$ protons. The instantaneous luminosity (L_{inst}) of LHC, which is proportional to the rate of collisions (and thus a critical collider parameter) can be expressed as

$$L_{inst} = \frac{N^2 f n_b}{4\pi \sigma_x \sigma_y}, \quad (5.1)$$

where N is the number of protons per bunch ($N \approx 1.15 \cdot 10^{11}$), f is the revolution frequency ($f \approx 11.245$ kHz), n_b is the number of bunches per beam ($n_b \approx 2800$), and σ_x and σ_y are the horizontal and vertical beam sizes at the interaction point ($\approx 20 \mu\text{m}$). The time integrated luminosity collected by the LHCb experiment, framework of this master thesis, is 3 fb^{-1} , 6 fb^{-1} and 9 fb^{-1} for Run 1, Run 2 and Run 3 (partial), respectively.

Another important quantity, pileup (μ), is the average number of interactions per single bunch crossing, which can be expressed as

$$\mu = \frac{L_{inst} \sigma_{inel}}{f}, \quad (5.2)$$

where σ_{inel} is the inelastic proton-proton cross-section ($\sigma_{inel} \approx 80$ mb at 14 TeV). Controlling this parameter is crucial for the even reconstruction, since a large pileup may significantly deteriorate the disentangling ability of decay of interest from the rest of the event. The pileup at LHCb is $\mu \approx 1.1$ and 1.5 for Run 1 and Run 2 respectively. For the present Run 3 $\mu \approx 5.3$.

The layout of the LHC collider complex with highlighted major experiments is shown in Fig. 6. The four main detectors, ATLAS, CMS, ALICE, and LHCb, are placed at

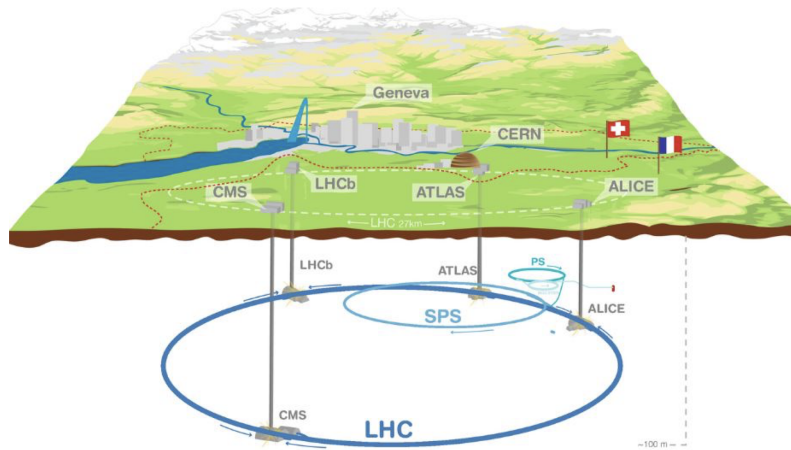


Figure 6: Schematic layout of LHC complex showing accelerators together with major experiments [7].

different interaction points around the LHC ring, each designed for a specific research

focus. ATLAS and CMS are general-purpose detectors designed to explore a broad spectrum of physics, including the search for the Higgs boson. On the other hand, ALICE is optimized to study the quark-gluon plasma, a state of matter believed to have existed just microseconds after the Big Bang, by colliding lead ions instead of protons. LHCb is a specialized flavor physics experiment studying decays of b and c quarks, investigating the differences between matter and antimatter particle decays, and also focusing on hadron spectroscopy.

6 The LHCb experiment

The LHCb forward spectrometer is one of the main detectors at the LHC accelerator at CERN, with the primary purpose of searching for new physics through studies of CP-violation and heavy-flavor hadron decays. It has been operating during all LHC Runs (Run 1 - Run 3) so far with very high performance, recording an integrated luminosity of 18 fb^{-1} at center-of-mass energies of 7, 8, and 13 TeV and delivering a plethora of accurate physics results and new particles discoveries [23].

The upgraded LHCb detector (Fig. 7), operational at present during the Run 3 of the LHC, has implied a major change in the experiment. The detectors have been almost completely renewed to allow running at an instantaneous luminosity five times larger than

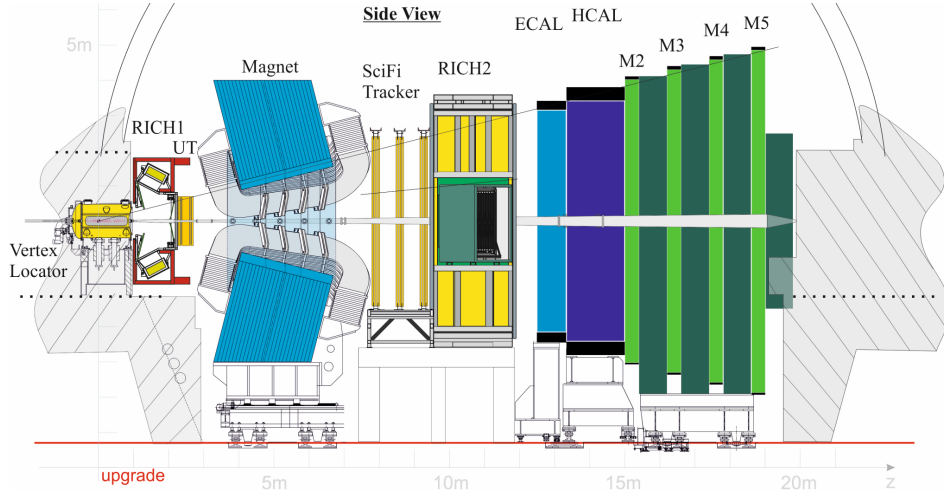


Figure 7: The new LHCb detector operating during the Run 3 [24].

that of the previous running periods, in particular using new readout architectures. A full software trigger executed on Graphic Processor Units (GPU) represents one of the main features of the new LHCb design, allowing the reconstruction and selection of events in real-time and widening the physics reach of the experiment [25]. The main characteristics of the new LHCb detector are detailed in [26], and summarised in the following. As compared to the previous detector [27], one of the most important improvements concerns the new tracking system, which is the key for this work. The subsystems of LHCb are:

1. **Tracking detectors**, designed to precisely reconstruct spatial track coordinates: VERTex LOcator (VELO), Upstream Tracker (UT), and Scintillating Fiber Tracker (SciFi).
2. **A dipole magnet**: which bends the trajectory of charged particles and enables momentum measurements.
3. **Particle Identification (PID) system**: designed for particle identification, differentiation, and energy measurement. The system includes Ring Imaging Cherenkov detectors (RICH1 and RICH2), muon chambers, and electromagnetic and hadronic calorimeters.

6.1 VERTex LOcator (VELO)

The VELO detector is responsible for the primary and secondary vertex reconstruction and track position measurements close to IP. The spatial resolution is less than typical decay lengths of b - and c -hadrons, i.e., $c\tau \approx 0.01 \text{ cm} - 1 \text{ cm}$, which is crucial for effective background rejection from heavy flavor signals. The detector itself was made of silicon micro-strip layers during Run 2, and it has been upgraded to a silicon hybrid pixel technology for Run 3.

The core technology of the new VELO is pixelated hybrid silicon sensors of $55 \mu\text{m} \times 55 \mu\text{m}$, which are arranged into 52 modules with 4 sensors each, and cooled by a bi-phase CO_2 microchannel system embedded in the silicon substrate. The VELO services have been redesigned reducing both the material budget and the inner radius of the VELO along the beamline. The modules are arranged into two movable halves, the Side C ($x < 0$) and Side A ($x > 0$). Both sides have a common z distribution but C-side modules are shifted 12.5 mm along the z axis to assure mechanical compatibility and sensor overlap when closed, providing a complete azimuthal coverage. A sketch of the VELO detector is shown in Fig. 8.

6.2 Upstream Tracker (UT)

The second tracker in LHCb, named Upstream Tracker (UT) is positioned between the RICH1 detector and the dipole magnet. It plays a critical role in charged-particle tracking [28]. The setup comprises four planes of silicon strip detectors and it is shown in Fig. 9. The planes are referred to as UTaX, UTaU, UTbV and UTbX. The strips in UTaX and UTbX plane are arranged vertically along the y -axis and in UTaU and UTbV are inclined at stereo angles of 5° .

The UT provides a preliminary momentum estimation for tracks with transverse momentum $p_T > 0.2 \text{ GeV}/c$, by using fringe magnetic field between the interaction region and the UT itself. This results in moderate precision ($\approx 15\%$) which allows to expedite

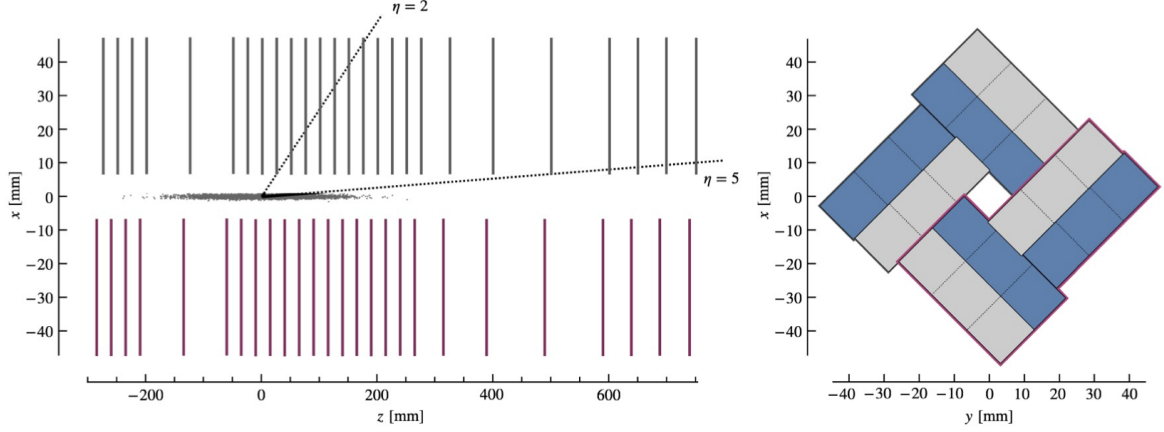


Figure 8: Left: A top-view on the $z-x$ plane at $y=0$ shows the luminous region z -extent and pseudorapidity acceptance ($2 < \eta < 5$). Right: A sketch presents the ASICs' standard layout around the z -axis in the closed VELO. ASICs are split between the upstream (grey) and downstream (blue) module faces. Side C modules are highlighted in purple in both images.

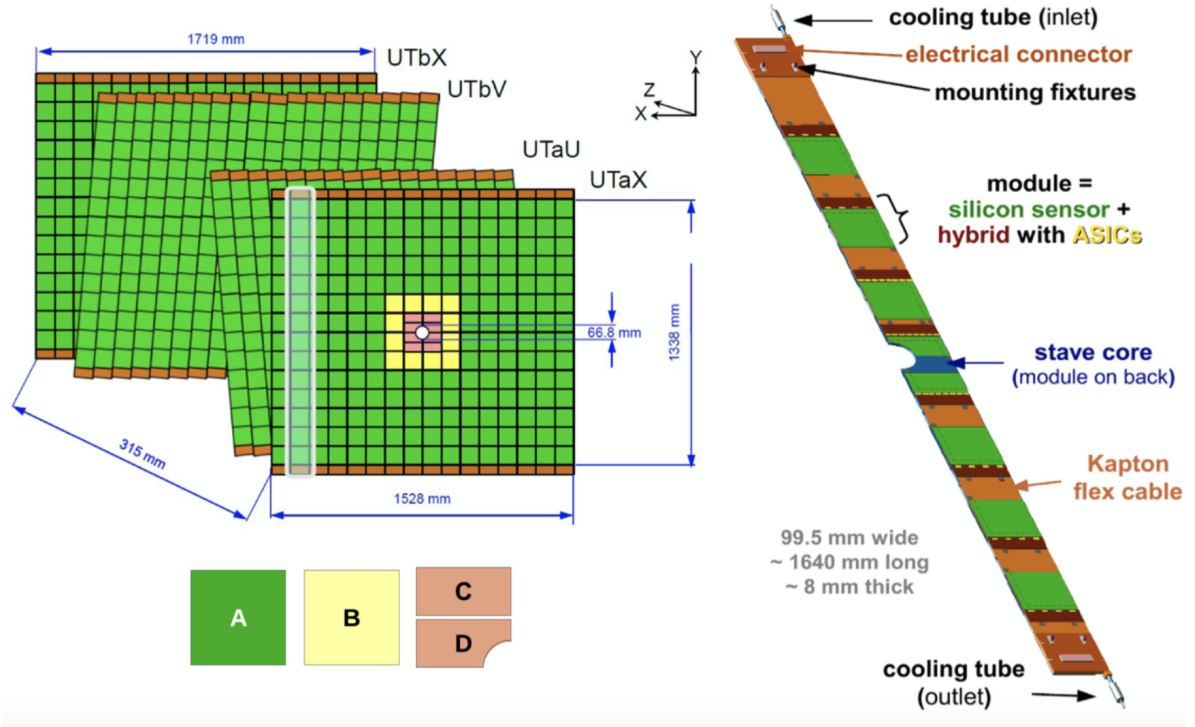


Figure 9: The configuration of the UT's four layers is illustrated. Distinct colors represent the various sensor types. On the right, the design of a UT stave is displayed [29].

the matching with Scintillating Fibre Tracker (SciFi) hits. Furthermore, the UT provides essential information about particles that decay after the VELO such as the long-lived K_S^0 and Λ .

6.3 Scintillating Fibre Tracker (SciFi)

The Scintillating Fibre Tracker (SciFi), the last LHCb tracker and the most innovative detector of the LHCb upgrade, is placed downstream of the LHCb dipole magnet as shown in Fig. 10. It uses the cutting-edge technology of long scintillating fibers. The detector is responsible for charged particle tracking and momentum estimation.

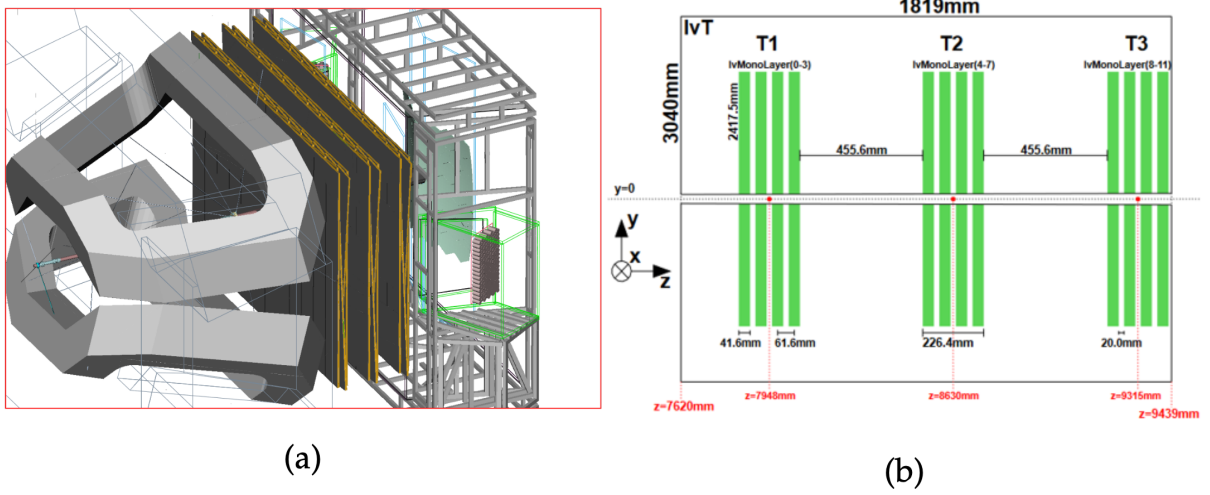


Figure 10: (a) The three stations of the SciFi are shown between the dipole magnet on the left and RICH2 on the right. (b) Sketch of the SciFi detector showing the three stations and the four layers in each station.

To meet the nominal LHCb acceptance, the tracker has to cover an area of roughly $6\text{ m} \times 5\text{ m}$ in the $x - y$ plane. The acceptance of the new SciFi detector ranges from approximately 20 mm from the beam pipe edge to distances of $\pm 3186\text{ mm}$ and $\pm 2425\text{ mm}$ in the horizontal and vertical directions, respectively. The detector relies on $250\text{ }\mu\text{m}$ diameter plastic scintillating fibers in multi-layered fiber mats, arranged in 12 detection planes across 3 stations (named T1, T2, T3) with four layers in an $x - u - v - x$ configuration. Such configuration means that the detection layers are oriented at (0 deg, +5 deg, -5 deg, 0 deg) relative to the vertical axis, which allows the determination of the particle trajectories in both x and y coordinates.

The stations are built from identical SciFi modules that are approximately 52 cm wide, spanning the full height. Figure 10 shows a sketch of the different stations. Each station has four layers with each layer having two independently movable structures, referred to as C-frames, on either side of the beam pipe. The scintillating fibers light signals are detected by 128-channel arrays of silicon photomultipliers (SiPM) with a channel pitch of $250\text{ }\mu\text{m}$. This detector is the most important in the context of the current master thesis.

6.4 Magnet

A dipole magnet, located between the UT and SciFi, induces a deviation in particle trajectory in the horizontal plane from which it is possible to extract its momentum. The integrated magnetic field between the UT and SciFi is 4 Tm.

The polarity of the magnet is reversed periodically to minimize possible systematic uncertainties due to the detector asymmetries, which average out by using each half of the data in a different configuration (i.e magnet polarity up and down). The magnetic field distribution is shown in Fig. 11.

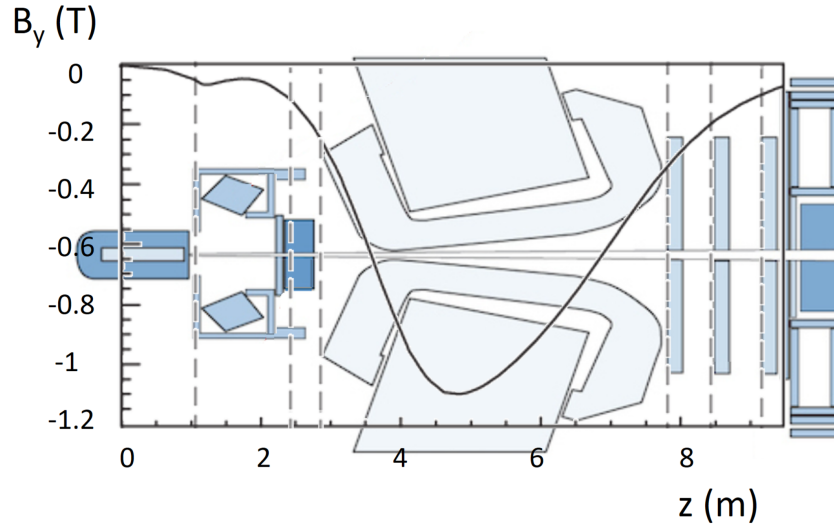


Figure 11: Distribution of the LHCb magnetic field as function of z . The VELO, RICH1, UT, magnet and the SciFi are superimposed.

7 Track description and types at LHCb

The existing convention on track types is based on the particular subdetectors the particle flies through. Main types are shown in Fig. 12, and defined as

- **VELO tracks** - formed by particles that hit only the VELO subdetector.
- **Upstream tracks** - formed by particles that pass through VELO and UT but do not reach SciFi.
- **Long tracks** contains hits from at least VELO and SciFi subdetectors. Presence of UT hits is optional. These are the main tracks used in physics analyses and at all stages of the trigger.
- **Downstream tracks** usually formed by decay products of K_S^0 and Λ particles, as they require only hits in UT and SciFi but not VELO. Recently the reconstruction of these tracks was implemented at HLT1 level [7].

- **Faraway tracks**, or T tracks ¹, they have hits from the SciFi only. The use of these tracks for physics analyses has been proposed recently [30]. The current work focuses on the reconstruction of *faraway* tracks at very early stages of the data taking.

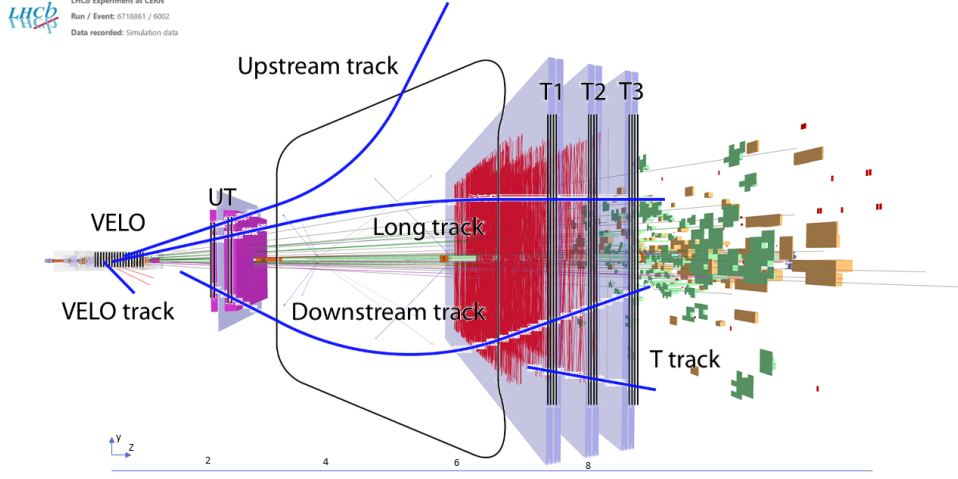


Figure 12: LHCb track types shown as a blue lines. The LHCb tracking detectors together with example calorimeter clusters are superimposed.

In LHCb, the coordinate system is adopted for the tracking system and is right-handed with axes denoted as x , y , and z :

- The z -axis is collinear with the beam pipe, originating at the collision point and extending through the detector.
- The x -axis, perpendicular to the z -axis, lies in the plane where charged particles deviate due to the magnetic field, termed as the bending plane or the $x - z$ plane. The axis is pointed towards the outside of the LHC ring.
- The y -axis is orthogonal to both the x and z axes, pointing upwards, and defines the non-bending plane, referred to as the $y - z$ plane.

7.1 Track description model

Particle tracks are described as a series of linear segments, where each segment is called track state, defined at a given z . This representation is based on the premise that over short intervals, the track can be approximated as a straight line despite the curvature introduced by the magnetic field. Each track state is characterized by a five-dimensional state vector, \vec{s} , and an associated covariance matrix. The state vector is defined as:

¹Along this work the proposed term *Faraway* is used instead of T-tracks, since it is found to be more descriptive.

$$\vec{s} = \begin{bmatrix} x \\ y \\ t_x \\ t_y \\ \frac{q}{p} \end{bmatrix}, \quad (7.1)$$

where x and y denote positions along the horizontal (x) and vertical (y) directions, t_x and t_y represent the tangents of the direction angles with respect to the z coordinate, defined as $t_x = \frac{\partial x}{\partial z}$ and $t_y = \frac{\partial y}{\partial z}$, and $\frac{q}{p}$ signifies the charge-to-momentum ratio, where q represents the charge and p denotes the momentum of the particle.

The covariance matrix, a 5×5 matrix, incorporates the uncertainties and correlations of the components of the state vector and plays a crucial role in track fitting and analysis. This basic common track model provides a unified representation of the track states across the different tracking systems of LHCb.

8 The LHCb trigger system

The trigger system is completely renewed for Run 3 due to the inability to meet the physics requirements with the setup used in previous runs [24]. It includes the removal of the hardware trigger, and the development of brand-new software-based trigger system (Fig. 13) that allows the real-time reconstruction of all events at a visible interaction rate of 30 MHz and reduced data volume from 4 TB/s down to ≈ 10 GB/s, which is suitable for permanent offline storage.

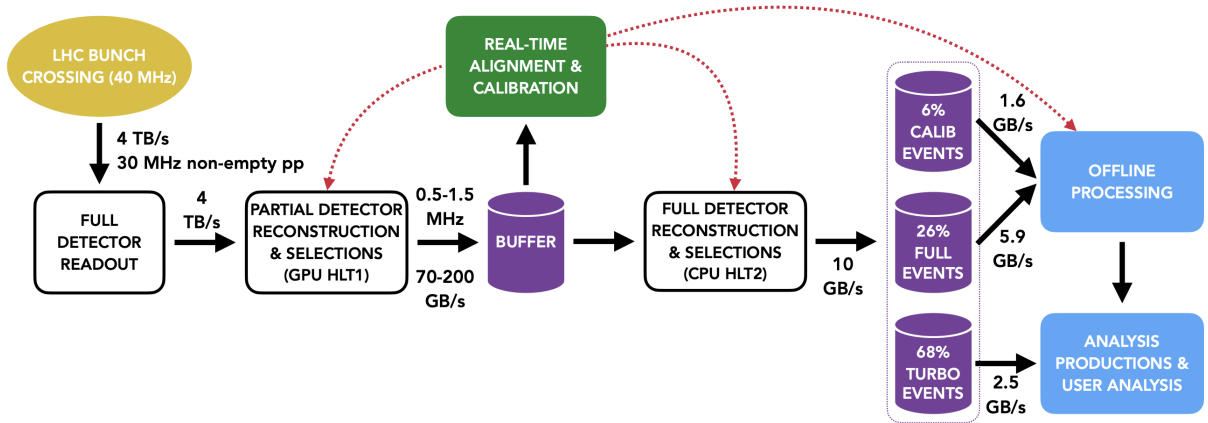


Figure 13: LHCb upgrade dataflow focusing on the real-time aspects [31].

The high rate of potentially interesting signals that can be at least partially reconstructed within the detector acceptance significantly complicates the reduction (400 times) of data flow. The trigger must fully reconstruct and pinpoint specific signals of interest, retaining only a select portion of the event's information [32]. This necessitates that the

trigger executes an offline-quality reconstruction, achieved by a near real-time alignment and calibration of the detector. The LHCb real-time analysis approach, initiated in Run 2 [33], underscores this demand [34].

8.1 High Level Trigger 1 (HLT1)

The HLT1 serves as the first filter in the LHCb trigger system, as shown in Fig. 13. The core idea of this trigger is reconstruction and selection tracking signatures of decays of interest. HLT1 is responsible for reduction of the incoming dataflow down to manageable levels, allowing data to be buffered for subsequent HLT2 processing. The event signal rates are predominantly driven by c -hadrons at nearly 1 MHz and b -hadrons at 300 kHz, both of which can be partially reconstructed within the LHCb’s acceptance parameters. Additionally, The LHCb physics program, including electroweak physics, quarkonia, semileptonic, and rare heavy decays, among others, significantly influences the event rate. The HLT1 design ensures its output rate does not theoretically surpass 2 MHz. Yet, practical constraints, such as the disk buffer capacity and HLT2 processing speeds, dictate this rate, as visualized in Fig. 13.

8.2 High Level Trigger 2 (HLT2)

The primary function of HLT2 is to carry out the full offline-quality reconstruction and selection of physics signatures. A sizable disk buffer is placed between HLT1 and HLT2 to serve as a temporary repository for data while real-time alignment and calibration are conducted. At HLT2, the fate of an event, whether it should be conserved, is determined by roughly $\mathcal{O}(1000)$ selection algorithms each individually tuned for a distinct signal topology or physics analysis. These algorithms also decide which components of the full event are to be committed to permanent storage. The reconstruction pipeline comprises four core components: charged particle pattern recognition, calorimeter reconstruction, particle identification, and a Kalman fit for tracking. To achieve the required computing throughput, tracks, neutral objects, and particle identification data are grouped into Structure-of-Array (SoA) data structures, enabling efficient parallel processing. Selection algorithms employ both rectangular-cut-based methods and techniques rooted in multivariate analysis or artificial intelligence.

9 Track reconstruction algorithms at HLT1

The existing track reconstruction algorithms at HLT1 are described in the following subsections. The first two, named *VELO* and *SciFi* track reconstruction, are designed to reconstruct track segments based only on the hit information in respective detectors.

On the other hand, the last two algorithms combine track segments from different sub-detectors in order to reconstruct a complete particle trajectory within LHCb.

9.1 *VELO* track reconstruction

As a first detector around the interaction point, VELO has to deal with huge number of hits coming from collisions. The huge LHCb event rate leads to around 1 billion of particle tracks per second coming from pp collisions. Composed of 52 planes of silicon pixel sensors encircling the interaction region, the primary function is the reconstruction of Primary Vertices (PVs) and the generation of initial track seeds. These seeds are then propagated through the other detectors of the LHCb for further processing.

The reconstruction of straight-line tracks begins with the generation of three-hit seeds triplets from successive layers, using the algorithm called **Search by triplet** [35]. These triplets are then extended to other layers, considering that prompt particles from pp collisions that travel through the detector are straight lines with a constant polar ϕ angle from the PV. To facilitate rapid reference during the combination of hits into tracks, the hits on each layer are sorted by their ϕ angle. Lastly, these initial *VELO* tracks are refined using a simple Kalman filter [36].

9.2 *SciFi* track reconstruction

The *SciFi* track reconstruction is part of several algorithms inside the **Allen** framework, namely the **Forward** [37] and the **HybridSeeding** [38]. While the **Forward** algorithm is designed to reconstruct *long* tracks, **HybridSeeding** is able to reconstruct the standalone *SciFi* tracks and, because of that, is very important in context of the current work.

The **HybridSeeding** algorithm for HLT1 on GPUs is an adaptation of the **HybridSeeding** algorithm implementation at HLT2 level based on CPUs. The algorithm is based on reconstructing tracklets in the $x - z$ plane (also the bending plane for tracks, the algorithm is called **Seeding_XZ**) and then confirming the candidates in the $x - y - z$ space by adding $u - v$ information (**Seeding_confirmTracks**).

9.2.1 Partial reconstruction in xz plane with **Seeding_XZ**

For every hit in the first x -layer of the T1, a small search window is opened in the first x -layer of T3, and all the hits in that window are matched to create two-hit combinations. The position and width of this search window are determined based on the assumption that the particle's origin vertex is (0,0,0) and its momentum $p_{min} > 3$ GeV/c. At this stage, the tracks are assumed to be straight lines in the bending plane. A sketch of the algorithm principle is shown in Fig. 14.

For every two-hit candidate, slope calculations are performed using the extrapolation of the doublets to ($x=y=z=0$). An initial track momentum assumption of $p_{min} > 3$ GeV/c

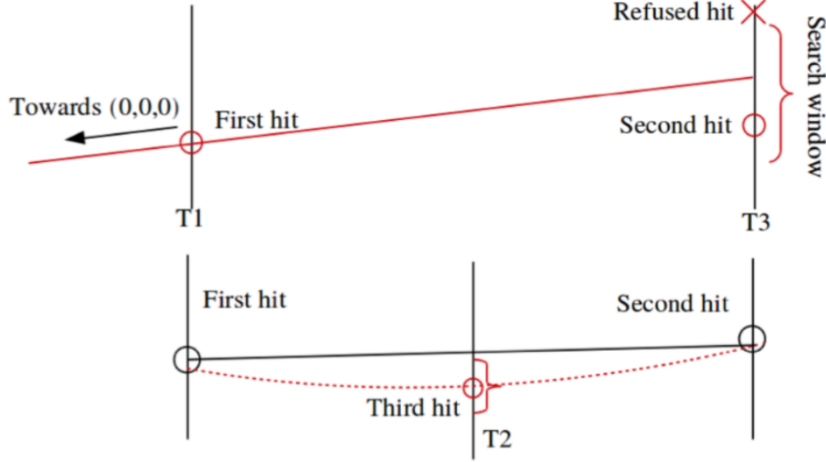


Figure 14: Illustration of the two- and three-hit searches in the $x - z$ plane..

for which the seeding is tuned is used to determine the size of the window in the first x -layer in T2. Due to the remaining magnetic field in the SciFi detector, tracks in the $x - z$ plane follow trajectories defined by the expression of the parabolic track model in Eq. 9.1.

$$x(z) = a_x + b_x \bar{z} + c_x \bar{z}^2 \left(1 + \frac{\Delta B}{B} \bar{z}\right), \quad (9.1)$$

where $\bar{z} = z - z_{ref}$, with $z_{ref} = 8525$ mm, and a_x , b_x , c_x are terms of the parabola that need to be determined. The variable $\frac{\Delta B}{B}$ is fixed using the simulated samples and represents the decreasing magnetic field along the z direction. This allows to define a tight search window for hits in the first x -layer in T2. Taking the bending into account, all the hits from the T2 first x -layer within the tolerance window are added to create three-hit combinations as depicted in Fig. 14. The three-hit combinations are fitted with a parabola track model with cubic correction term.

The three-hit combination's parabolic trajectory is subsequently projected onto the remaining three x -layers, and any detected hits within a permissible window of 1 mm are incorporated. The parabola is then extended to the remaining layers. The candidates with at-least two additional hits from remaining layers, i.e. at least five out of six possible hits, are selected, and a track fit is performed in the $x - z$ plane. Each track candidate is assigned a score based on the number of hits and χ^2 value. A GPU-optimised shared memory $\mathcal{O}(N)$ voting algorithm is used for clone tracks removal before the next step of adding y -information.

9.2.2 Charge-momentum estimation and tolerance windows

The xz -seeding utilises tolerance windows, which are fine-tuned using simulated $B_s^0 \rightarrow \phi\phi$ decays. These windows are parameterized basing on momentum and other topological variables. For efficient GPU seeding, an initial track momentum assumption of $p_{min} >$

3 GeV/c was adopted. Tracks can be approximated as originating from the point (0,0,0). The trajectory of a track can be predicted basing on its first hit in the detector. The relationship between this back-propagated x and q/p value for *long* tracks is modeled as

$$\frac{q}{p} = f(x_0) = a|x_0| + bx_0^2, \quad (9.2)$$

with specific parameters derived from simulations. The difference between the measured and predicted hit position in the T3 layer is proportional to x_0 . Using the $q/p = f(x_0)$ model, a momentum cut can be translated into a tolerance on this difference. The tolerance window's limits are then calculated, and over 99% of hits from tracks with $p > p_{min}$ fall within this window.

The third hit's deviation from the expected line provides another measurement of the track's q/p . This deviation is proportional to the track's quadratic coefficient. This tolerance is equivalent to a momentum measurement using only the residual magnetic field inside the SciFi detector. The distribution of this deviation as a function of q/p shows that most tracks follow a linear relationship, but some deviate due to factors like energy loss or different integrated fields. An additional correction factor, α_{corr} , is introduced to account for charge asymmetry as a function of the initial hit position. This factor is modeled as a function of momentum, and its parameters are derived from fits to simulated sample. The established tolerances, including the α_{corr} correction, are designed to encompass 99% of the tracks

9.2.3 Adding uv information and confirmation

In the case of a specific layer at a location $z = z_0$ and tilted at an angle θ , a measurement at $x = x_0$ can be converted into a y_0 measurement for a track with a given $x(z)$ equation, as expressed by:

$$y_0 = \frac{x(z_0) - x_0}{\tan(\theta)}. \quad (9.3)$$

Given that the magnetic field in the SciFi region primarily aligns with the y direction, trajectories are expected to follow straight lines in this direction. Based on the assumption that tracks originate from the origin, the y slope, denoted as t_y , should remain constant.

Consequently, for each parallel $x - z$ track considered, every hit of an initial layer is examined, and the associated t_y is computed. This value is then used to establish small tolerance windows in all other layers, and the hit nearest to the extrapolated position is collected. With each addition of a hit to the combination, the t_y value is updated.

Ultimately, a maximum of one combination per first hit considered is constructed. These combinations are then fitted, and the fit quality, along with the number of hits, is employed to select the candidate. Finally, a second iteration is performed, designating another layer as the initial layer, to compensate for hit inefficiencies. Tracks with a

combined total of 10 hits or higher from x and uv layers are accepted and a linear model in y is used to calculate track parameters. The resulting resolution in track slopes made with Minimum Bias² MC³ sample is shown on Fig. 15. The candidates with best χ^2 are confirmed as *SciFi* tracks. All these operations are carried out in parallel for all the xz candidates.

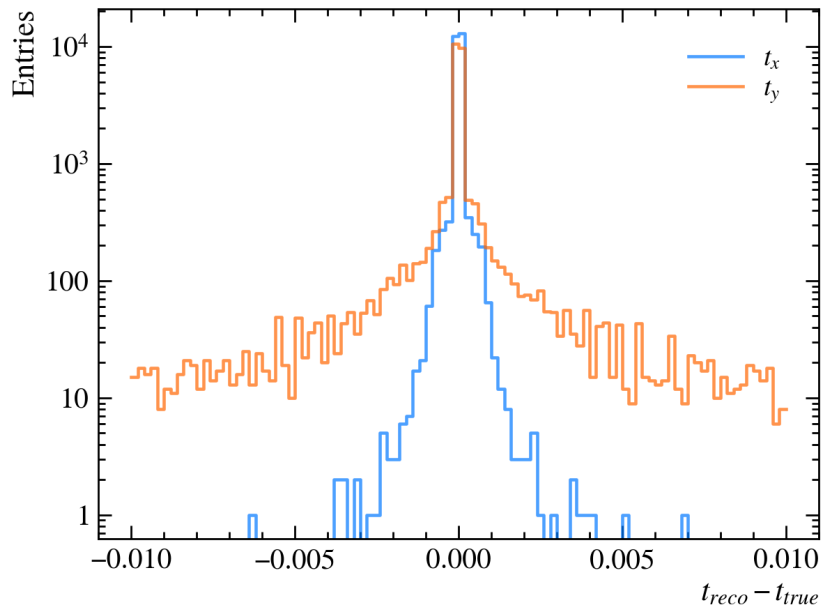


Figure 15: Histogram of reconstruction errors in track slopes t_x and t_y with respect to true values, made using Minimum Bias MC sample.

In the previously outlined process, executing the xy seeding twice tends to create a multitude of clones. To address this, a voting algorithm is introduced, which calculates a score for each hit included in the tracks, basing on the following formula:

$$s = 1000\chi^2 + c_x \quad (9.4)$$

where χ^2 provides the fit quality of the track, and c_x is the parabola term of the trajectory in x . If this calculated score is less than the current score attributed to a hit, the new score will be assigned to that hit.

The term c_x is included in our scoring equation due to the need for a deterministic way to break ties when two track χ^2 values are the same. The selection of c_x is specifically motivated by the intention to favour tracks with higher momentum over those with lower momentum, thereby prioritizing tracks that are more likely to come from b -hadrons decays.

Afterwards, a second round of evaluations on the tracks is conducted. A track will be preserved if a minimum of four hits are associated with this specific track score. This operation is designed to run in parallel over the tracks, optimizing the computational

²Minimum Bias simulation sample corresponds to the running conditions expected in Run 3.

³MC stands for Monte Carlo method and is used for simulation of events.

efficiency.

9.3 Long track reconstruction

Two different algorithms were developed for *long* track reconstruction, named **Forward** and **Velo-SciFi Matching**. The first one relies on the extrapolation of *VELO* segments towards the SciFi plane, and sequential hit assignment afterwards. This does not require any standalone *SciFi* track segments. On the other hand, within the **Velo-SciFi Matching** algorithm, *VELO* tracks are matched to the *SciFi* track seeds reconstructed by the standalone seeding algorithm described above to create *long* tracks. This is shown in Fig. 16. The momentum kink depends on the integrated magnetic field along the path

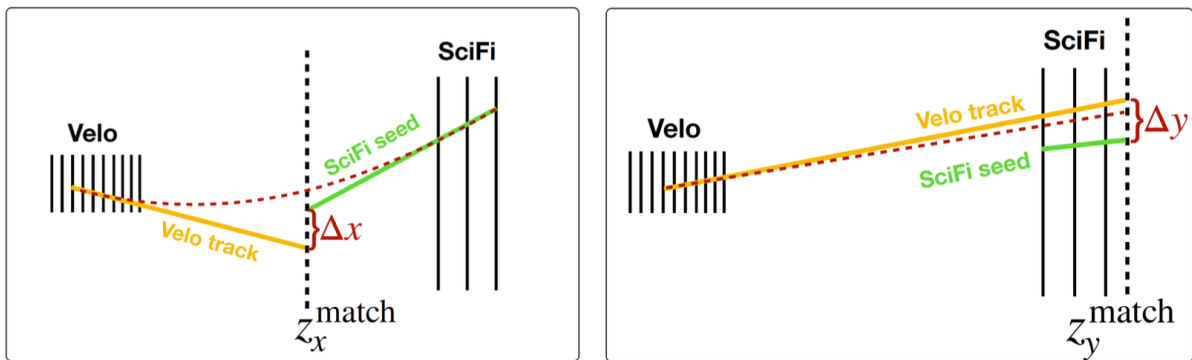


Figure 16: Illustration of the work principle of the **Matching** algorithm in the (left) $x - z$ plane and (right) $y - z$ plane [39].

followed by the track and is calculated using MC simulations taking the magnetic field map of LHCb detector into account. The ideal position to align the two track segments in a straight line model fluctuates basing on the momentum of the track. Hence, the z -position of the kink, termed z_x^{match} , is not static but rather includes the parameterisation of the magnetic field.

Best candidates are selected using a χ^2 minimization strategy in Δx , Δy and Δt_y . Further, a clone-killing procedure is applied wherein the tracks that share a *VELO* track are compared and only the ones with the best χ^2 are kept.

The global efficiency of **Velo-SciFi Matching** algorithm is more than 80% and for low momentum tracks is around 60%. The fake track rate is below 5% and the momentum resolution is below 1% for most of the tracks. The HLT1 throughput drop is around 3% [7].

9.4 Downstream track reconstruction

The **Downstream** track reconstruction algorithm is based on the extrapolation of *SciFi* tracks to the UT detector through the LHCb dipole magnet. The extrapolation can be modeled as a sharp change in direction, akin to a *kink*, at a specific position along the z -axis. This position is termed as the “magnet point” and is denoted as z_{Magnet} . Using

this point one can derive equations for x_{Magnet} and y_{Magnet} coordinate of the kink point:

$$\begin{aligned} z_{Magnet} &= \alpha_0 + \alpha_1 t_y^2 + \alpha_2 t_x^2 + \alpha_3 q/p + \alpha_4 |x_{SciFi}| + \alpha_5 |y_{SciFi}| + \alpha_6 |t_y| + \alpha_7 |t_x| \\ y_{Magnet} &= (y_{SciFi} + dy) + t_{y_{mag}} (z_{Magnet} - z_{SciFi}) \\ x_{Magnet} &= x_{SciFi} + t_x (z_{Magnet} - z_{SciFi}) \end{aligned} \quad . \quad (9.5)$$

Here, $t_x = \frac{dx}{dz}$, $t_y = \frac{dy}{dz}$, x_{SciFi} and y_{SciFi} are the slopes and coordinates of the track state in the last SciFi station, respectively. The initial signed track momentum estimate is based on *SciFi* track parameters and is denoted as q/p . The coefficients $\alpha_0 - \alpha_7$ are determined using MC simulations.

Using the previous extrapolation, the search windows in each of the UT stations are defined in order to search for the corresponding hits. Once hit assigning process is done, the final track fit is performed. The last step is a fake track killer. Tracks originating from spurious hits in the detector are suppressed by a neural network (NN) with a unique hidden layer [7].

The momentum resolution of *downstream* tracks is around 5%. The global efficiency of the algorithm is close to 70% and the fake rate does not exceed 23% for most of the decay channels. The HLT1 throughput drop is around 4% [7].

10 Studies of sensitivity to BSM particles

The impact of the **Downstream** algorithm on the LHCb physics performance was studied in [25]. It was concluded that the **Downstream** setup hugely increases the LHCb physics possibilities towards the exploration of a diverse range of LLPs, competitive with the exploration potential of other LHC-based experiments like FASER2.

The complete dataset from LHCb up to Run6 is expected to allow to probe Heavy Neutral Leptons (HNLs) with masses up to approximately 20 GeV/ c^2 , as well as dark photons and B - L mediators with masses of around 1 GeV/ c^2 . Moreover, this approach extends the search to Higgs-like scalars with lifetimes exceeding those accessible by the current LHCb search strategies, and to axion-like particles with various couplings.

Sensitivities of LHCb experiment with/without **Downstream** and FASER2 to example Higgs-like scalars and HNLs are shown in Fig. 17. Further enhancements in sensitivity can be achieved by enlarging the effective decay volume and incorporating the possibility of reconstructing final states comprising exclusively photons, contingent upon the development of new triggers. The former may be achieved by the introduction of the **Faraway** reconstruction algorithm, which is the main topic of the current work.

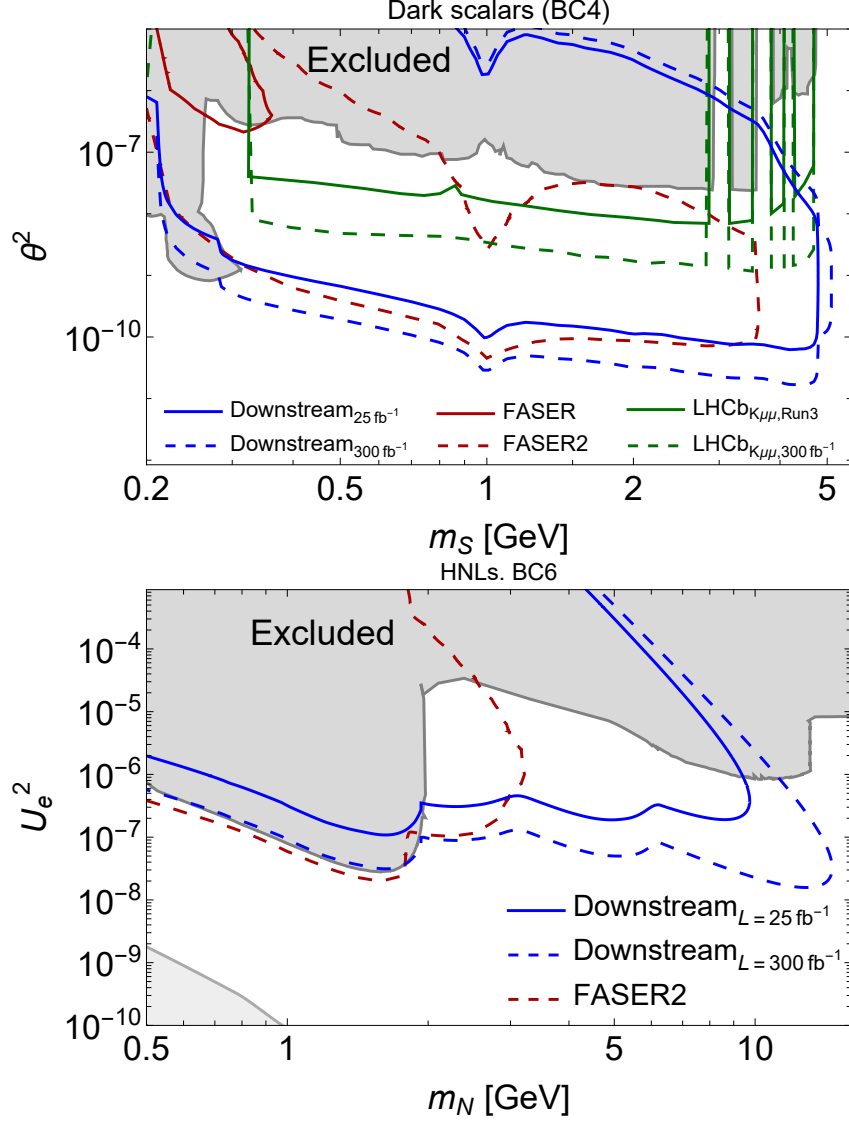


Figure 17: Sensitivity to Higgs-like scalars within model BC4 (the left panel) and HNLs coupled solely to ν_e (the right panel). [25]. The blue line represents the LHCb sensitivity region with the new **Downstream** reconstruction algorithm. The excluded parameter space is taken from [40, 41, 42].

11 Faraway reconstruction algorithm

The large number of *SciFi* tracks per event ($\approx 10^2$) together with the poor momentum resolution ($\approx 15\%$, Fig. 18) makes the selection process challenging, especially with one-track trigger line algorithms. Therefore, two-track trigger lines are favoured from the selection point of view, but they require the development of an efficient algorithm for track extrapolation through the magnetic field and vertex reconstruction. The extrapolation is discussed in the current section, while vertex reconstruction and selection are described in the following sections

11.1 *SciFi* track segments and momentum resolution

The *HybridSeeding* is the only algorithm that provides standalone *SciFi* tracks and, therefore, it is used as a starting point for the *Faraway* reconstruction algorithm. Given the fact that *SciFi* hits are the only available tracking information, the momentum estimation of each track is obtained from individual hit deviation from linear trajectory due to the remaining magnetic field in the *SciFi* region.

Using the *HybridSeeding* track model (Eq. 9.1), one can calculate the curvature of the trajectory in the xz plane:

$$R(z) = \frac{(1 + x'(z)^2)^{\frac{3}{2}}}{|x''(z)|} = \frac{((b_x + c_x \bar{z}(3d_x \bar{z} + 2))^2 + 1)^{3/2}}{2|3d_x \bar{z} c_x + c_x|}, \quad (11.1)$$

where $d_x = \frac{\Delta B}{B}$. Then the charge over momentum fraction can be approximated as:

$$\frac{q}{p} = \frac{C}{R(\bar{z}_{qop})}, \quad (11.2)$$

where C and \bar{z}_{qop} are constants, estimated using MC simulations ($\bar{z}_{qop} = 0$). The latter is the z coordinate, at which the q/p fraction is estimated. The choice of these constants was done in a way that minimizes the error of the reconstructed q/p . The resulting momentum resolution *vs* particle momentum is shown in Fig. 18.

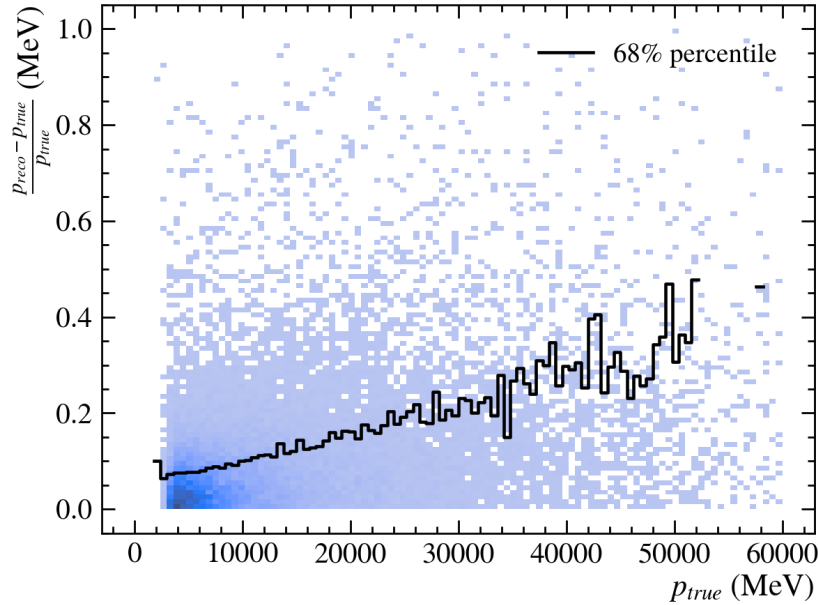


Figure 18: Relative momentum resolution of *faraway* tracks *vs* momentum value. The black line represents the 68% percentile for each momentum bin.

11.2 Extrapolation model

In order to reconstruct the vertices formed by *faraway* tracks, one has to extrapolate tracks through a highly nonlinear magnetic field. The classic approach to this problem is to involve the Runge-Kutta method [43]. However, this approach requires knowing the map of the magnetic field at all points of the detector volume, which has to be stored in the memory. This would lead to numerous memory read accesses, which, together with a considerable number of iterations (≈ 10), may significantly slow down the HLT1 processing.

Instead, it is decided to try to avoid algorithms that require frequent access to the memory. In general, the track extrapolation model may be written as follows:

$$x(z) = x_0 + t_x \bar{z} + \frac{q}{p} f(\bar{z}, \vec{s}_{SciFi}), \quad (11.3)$$

where \vec{s}_{SciFi} is the track state vector at the end of SciFi stations, f is an unknown function of \bar{z} and \vec{s}_{SciFi} (from now onwards f is named as trajectory function).

This equation contains two different parts: linear (the behaviour of the track in the absence of the magnetic field) and nonlinear, proportional to $\frac{q}{p}$ (which contains the whole effect of the magnetic field on the particle's trajectory).

The trajectory function can be estimated in two ways, using standard LHCb MC samples and with a dedicated simulation setup. Both are discussed below.

11.3 Trajectory function studies using standard LHCb MC samples

The only true MC information regarding particle trajectory in standard LHCb MC samples is the origin vertex position (\vec{x}_{ovtx}), momentum vector (\vec{p}_{ovtx}) at the same point of space, and hits in the detectors, left by this particle. By the reconstruction of these hits from the SciFi detector using a similar algorithm to **HybridSeeding**, one can estimate the true position and momentum vector at $\bar{z} = 0$. With this information, one may estimate the value of the trajectory function and its derivative using the definition 11.3:

$$\begin{aligned} f(\bar{z}_{ovtx}, \vec{s}_{SciFi}) &= (x^{ovtx} - x^{sf} - t_x^{sf} \bar{z}) \left(\frac{q}{p} \right)^{-1}, \\ \left. \frac{\partial f(\bar{z}, \vec{s}_{SciFi})}{\partial \bar{z}} \right|_{\bar{z}=\bar{z}_{ovtx}} &= (t_x^{ovtx} - t_x^{sf}) \left(\frac{q}{p} \right)^{-1}, \end{aligned} \quad (11.4)$$

where x^{sf} , t_x^{sf} - position and slope along x coordinate at $\bar{z} = 0$ (at the end of SciFi stations), x^{ovtx} , t_x^{ovtx} - position and slope at origin vertex. Within this approach, one can estimate one point per one particle, so in order to study the $f(z)$ and $f'(z)$ dependencies, one needs to use a large number of tracks, coming from the MC sample (see Fig. 19). The last step is the fitting of the trajectory function. Given the fact that $f(z)$ represents

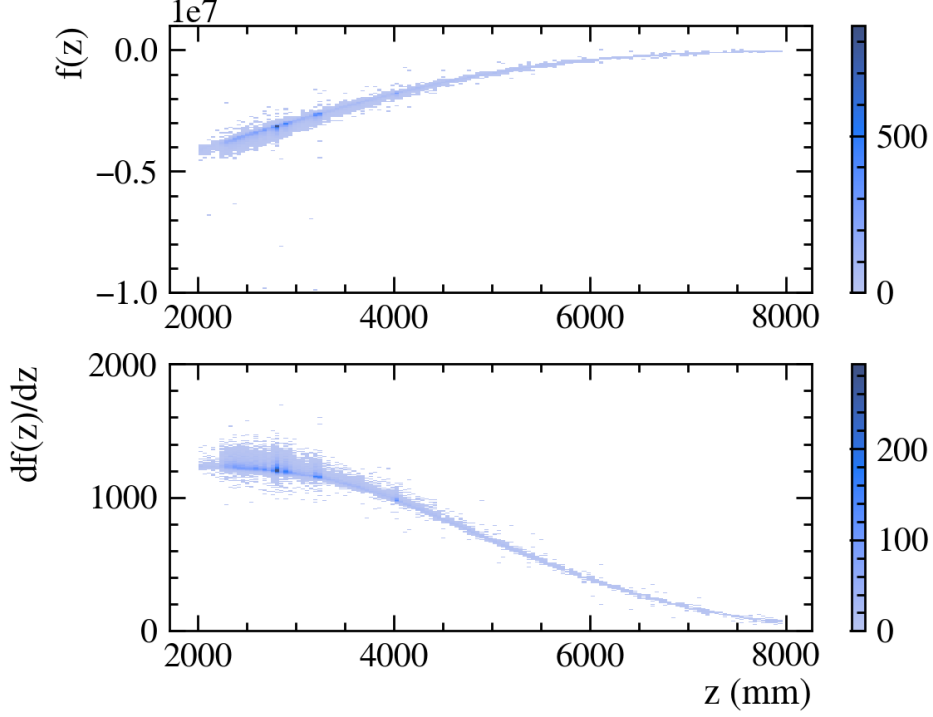


Figure 19: Trajectory function (top) and its derivative (bottom) studies using LHCb Minimum Bias MC samples.

a magnet effect on the particle trajectory and that the magnetic field is highly nonlinear, the exact analytical expression for $f(z)$ is not important. As an example, the following expression is proposed:

$$f'(z) = \begin{cases} \frac{a}{1+e^{-b(\bar{z}-c)}}, & \text{if } \bar{z} \leq \bar{z}_c, \\ 4g\bar{z}^3 + 3f\bar{z}^2 + 2e\bar{z} + d, & \text{otherwise,} \end{cases} \quad (11.5)$$

where a, b, c, d, e, f, g - some constants, determined from MC. The function $f(z)$ is defined as an indefinite integral of Eq. 11.5. In addition, it is ensured that the $f(z)$ is continuous and smooth up to the second order, as $f'(z)$ determines the trajectory slope and has to be smooth. However, this function does not take into account the non-homogeneity of the magnetic field along x and y axes. The latter leads to significant asymmetric errors in extrapolation, as shown in Fig. 20.

While studies with existing MC samples are fast and do not require big-time investment, it is very important to track material interaction effects within detectors, as they can significantly affect the observable trajectory function $f(z)$. One of the ways to take those effects under control is to remove the detector material from the simulation, as described in the next section.

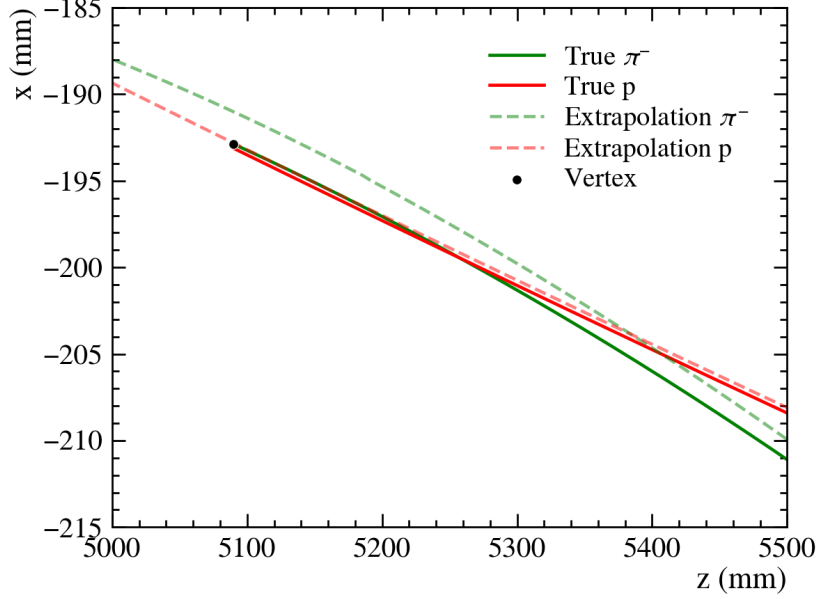


Figure 20: The validation of the extrapolation 11.5 for $\Lambda \rightarrow p\pi^-$, done with dedicated simulation method as described in section 11.4. The solid line represents true particle trajectories around the vertex, while the dashed represents extrapolated true SciFi states \vec{s}_{SciFi} with trajectory function 11.5. The deviation of softer π^- trajectory extrapolation from the true one may be caused by the non-homogeneity of the magnetic field in the outer parts of LHCb detectors, the particle flies through.

11.4 Trajectory function studies using a dedicated simulation setup

An alternative way to find functions $f(z)$ and $f'(z)$ is using dedicated simulation samples, that will allow precise study of trajectory functions. In the sample, particles should be simulated without any detector material to avoid an impact of unwanted material interactions, as they can be taken into account as extrapolation uncertainties later. In addition, the particle position should be stored on every simulation step, which allows studies of a complete trajectory function with only one particle using the same Eq. 11.3. A set of estimated trajectory functions and their derivatives is shown in Fig. 21.

The above-mentioned approach allows unbiased studies, as it eliminates the possibility of favouring specific SciFi states \vec{s}_{SciFi} (for example, from Minimum Bias distribution), as the generation can be done from any possible starting state.

The technical implementation of corresponding simulations is based on a particle gun (an object, that can shoot any particle in the desired direction from a given starting point). An example of particle trajectories from the same starting position and energy E but in a different direction is shown in Fig. 22.

In order to perform regular logging of particle trajectory and \vec{p} , a series of Geant4 [44] volumes with *OUTER_SPACE*⁴ material are created. This forces the Geant4 to perform a simulation step on each volume boundary. The logging logic is implemented inside

⁴*OUTER_SPACE* material represents empty space.

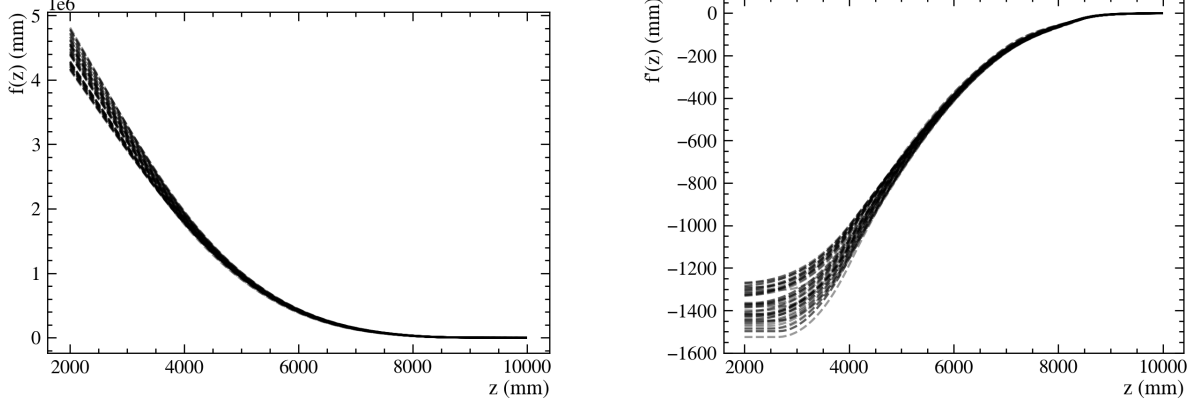


Figure 21: A set of trajectory functions (left) and its derivatives (right) evaluated using a dedicated simulation technique. The particles used for the simulation are π^\pm , with energy E from 2.5 GeV/c to 10 GeV/c. The initial position is at the SciFi plane in z and varies from -2 m to 2 m with step 0.5 mm in both x and y coordinates. The initial direction of the particle is randomly chosen across the ones that point into the UT plane.

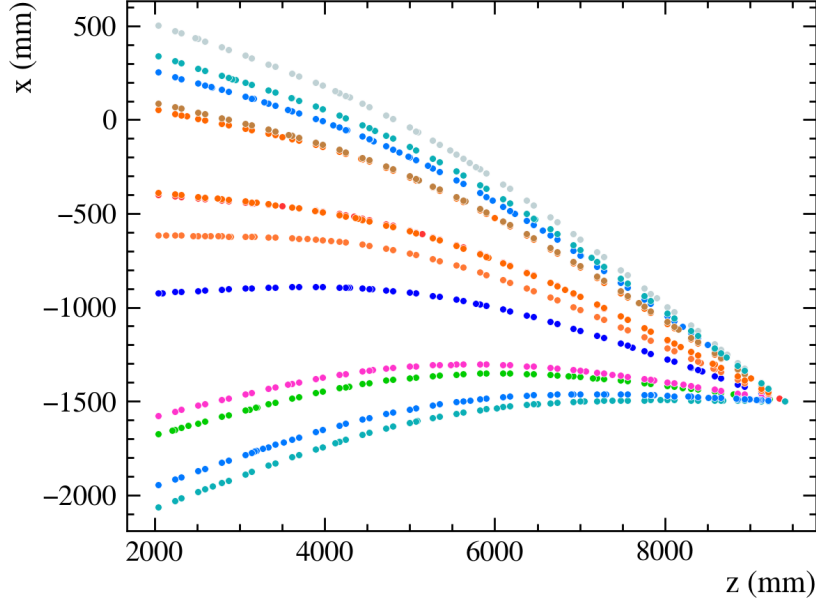


Figure 22: Particle gun demonstration. The π^- particles are shooter from the end of the SciFi detector in an upstream direction. Particles are killed in the UT plane $z = 2000$ mm. The simulation is done without taking into account the detector material.

`G4TrackingManager` algorithm which is responsible for track processing.

The evaluation of the final trajectory function is in progress at the moment of writing this thesis, as the above-mentioned approach allows the derivation of not only dependency of \bar{z} but an initial SciFi state \vec{s}_{SciFi} as well. This is described in more detail in Sec. 17.1

12 Vertex reconstruction algorithm

The vertex reconstruction is done by estimation of the point in space, at which the distance between two tracks is minimal (distance of closest approach, DOCA). In general, one may write such distance in xy plane (3^{rd} dimension is omitted for performance reasons):

$$D(z) = (x_A(z) - x_B(z))^2 + (y_A(z) - y_B(z))^2, \quad (12.1)$$

where $x_{A,B}(z)$, $y_{A,B}(z)$ - coordinates of the track A and B . This function can be minimized in z , and z_{min} may be treated as vertex z_{ovtx} coordinate. The other two coordinates can be then estimated as:

$$\begin{aligned} x_{ovtx} &= \frac{1}{2}(x_A(z_{ovtx}) + x_B(z_{ovtx})), \\ y_{ovtx} &= \frac{1}{2}(y_A(z_{ovtx}) + y_B(z_{ovtx})). \end{aligned} \quad (12.2)$$

However, given the different SciFi tracking resolutions along x and y axes, the corresponding $x_{A,B}(z)$ and $y_{A,B}(z)$ functions have different errors. In order to take this fact into account, one may try to introduce a weighted function $D_w(z)$:

$$D_w(z) = \frac{(x_A(z) - x_B(z))^2}{\sigma_x^2(z)} + \frac{(y_A(z) - y_B(z))^2}{\sigma_y^2(z)}, \quad (12.3)$$

where $\sigma_x(z)$ and $\sigma_y(z)$ are the extrapolation errors in x and y dimension respectively. These functions can be estimated using MC simulations. The comparison between the two methods is shown in Fig. 23. It was decided to proceed with the unweighted version of the $D(z)$ function, as the differences between them are small.

13 Fake vertex killer

In order to remove fake vertices, a NN-based filter was developed. It consists of one fully connected network with a single hidden layer. It is trained using a Minimum Bias MC sample and is using the following input variables:

- Daughter tracks momentum p , transverse momentum p_T and quality χ^2 .
- Absolute value of distances between daughter tracks in x and y coordinate at the vertex $z = z_{ovtx}$.
- The closest distance between daughter and mother tracks and point (0,0,5000 mm). This reference point was chosen empirically.
- Vertex z coordinate.
- The closest distance between the mother track and (0,0,0). Usage of this variable ensures that particles are coming from IP.

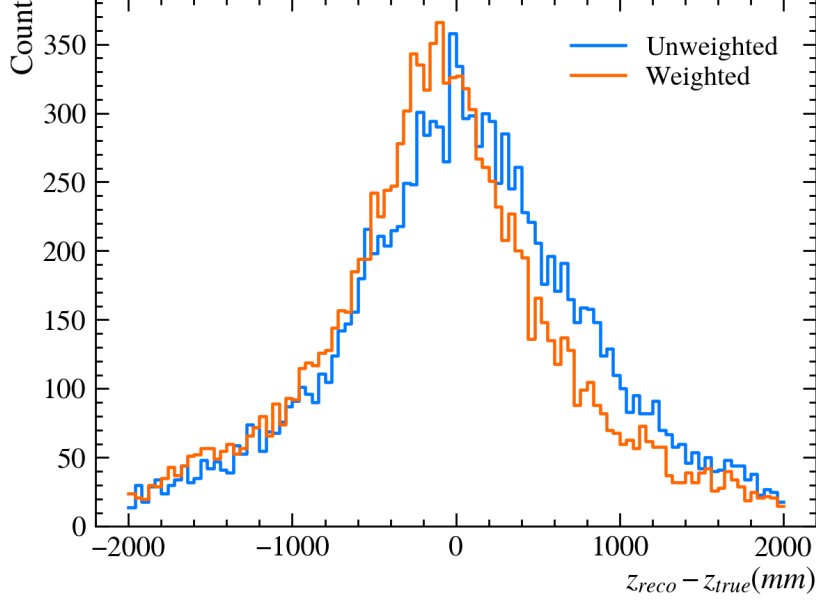


Figure 23: Histogram of reconstructed z_{ovtx} deviation from true value, made with Minimum Bias sample. The blue line represents reconstruction with unweighted function $D(z)$, while the orange one with weighted $D_w(z)$.

However, it is very difficult to distinguish between fake tracks and real particles coming from $z_{ovtx} < 5000$ mm region due to insufficient precision in *faraway* track parameters measurement (Fig. 24, left). Therefore, it was decided to introduce a prefiltering of composite candidates with a requirement, that particles originate from the region after $z = 5000$ mm to simplify the selection process.

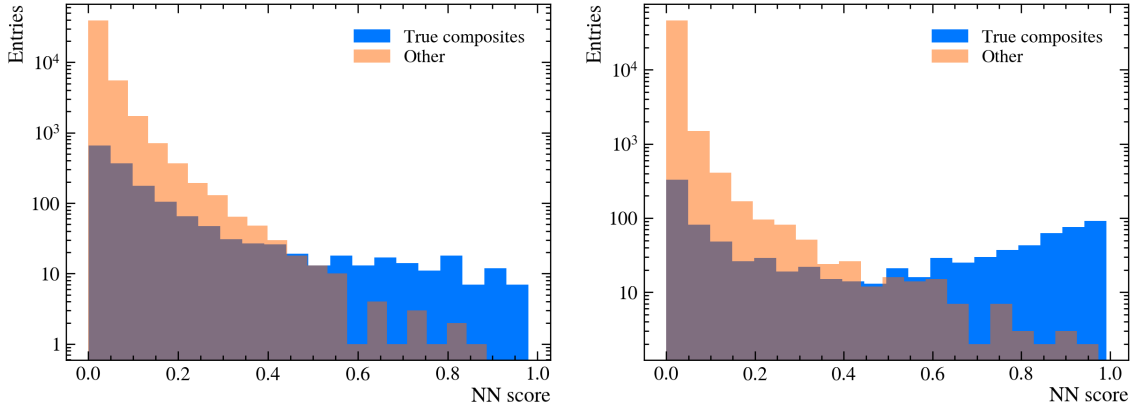


Figure 24: Neural network output for real (blue) and fake (orange) composite particles. On the left-hand side no prefiltering is applied, while on the right-hand side, a cut $z_{ovtx} > 5000$ mm is enforced. It is important to highlight that the plots are done on a logarithmic scale, and therefore even the smallest visual differences are not small. The plot is done using the Minimum Bias LHCb sample.

The output of the NN for real and fake composite particles is shown in Fig. 24. The fake rejection rate is 99.86% if the output score is larger than 0.5 and 99.99% if the score

is larger than 0.9. The corresponding efficiencies for the two cases are 41.8% and 15.5% respectively. The mass plots for composite particle candidates, that passed the fake killer NN, are shown in Fig. 25. It is worth highlighting that the combinatorial background has a flat shape, which, apart from the usual loss function analysis, proves that the NN learning is done correctly.

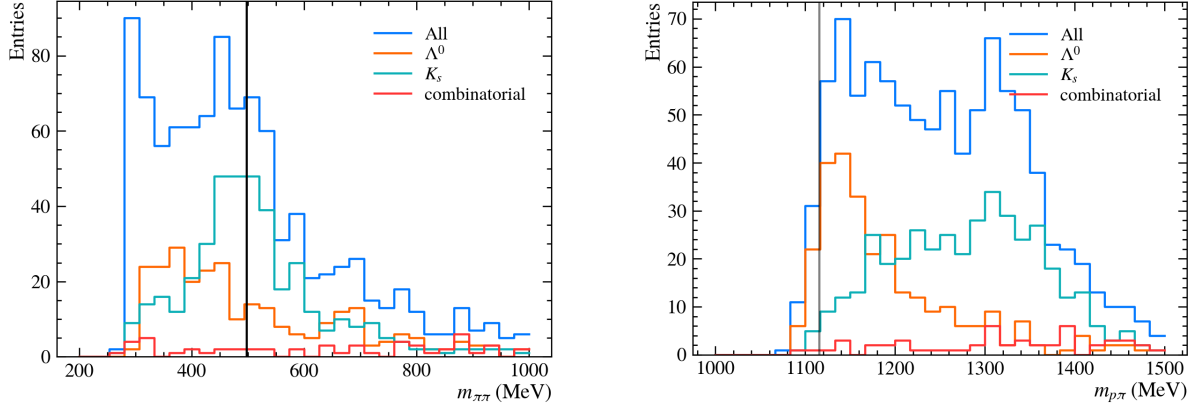


Figure 25: Mass distributions of composite particle candidates, that passed fake killer NN with cut 0.4. The color represents different true categories, orange for Λ , green for K_S^0 and red for combinatorial background.

14 Selection of particle candidates

The final selection of composite particle candidates is done with rectangular-cut based trigger lines for both Λ and K_S^0 hadrons. The selection cuts are determined as 95 % percentile of the corresponding distributions, as shown in Fig. 26 for Λ line and Fig. 27 for K_S^0 one. The mass distributions, made with Minimum Bias candidates that passed the selection line are shown in Fig. 28.

The total **Faraway** algorithm efficiency for $J/\psi \rightarrow \Lambda \bar{\Lambda}$ decay channel is 6% (while the one for the **TrackMVA**⁵ algorithm is 2%). For the $\Lambda_b^0 \rightarrow (J/\psi \rightarrow \mu^+ \mu^-) \Lambda$ decay channel the efficiency is 37% for **Faraway** case and 36% for **TrackMVA** case.

15 Algorithm implementation

The implementation of the algorithm in CUDA-based **Allen** framework is done in several steps each representing a separate LHCb **Gaudi** algorithm (and therefore CUDA kernel), that are glued together during **Allen** initialisation. The main steps are

- Creation of particle candidates using *SciFi* track segments.

⁵**TrackMVA** algorithm is used for *long* track selection.

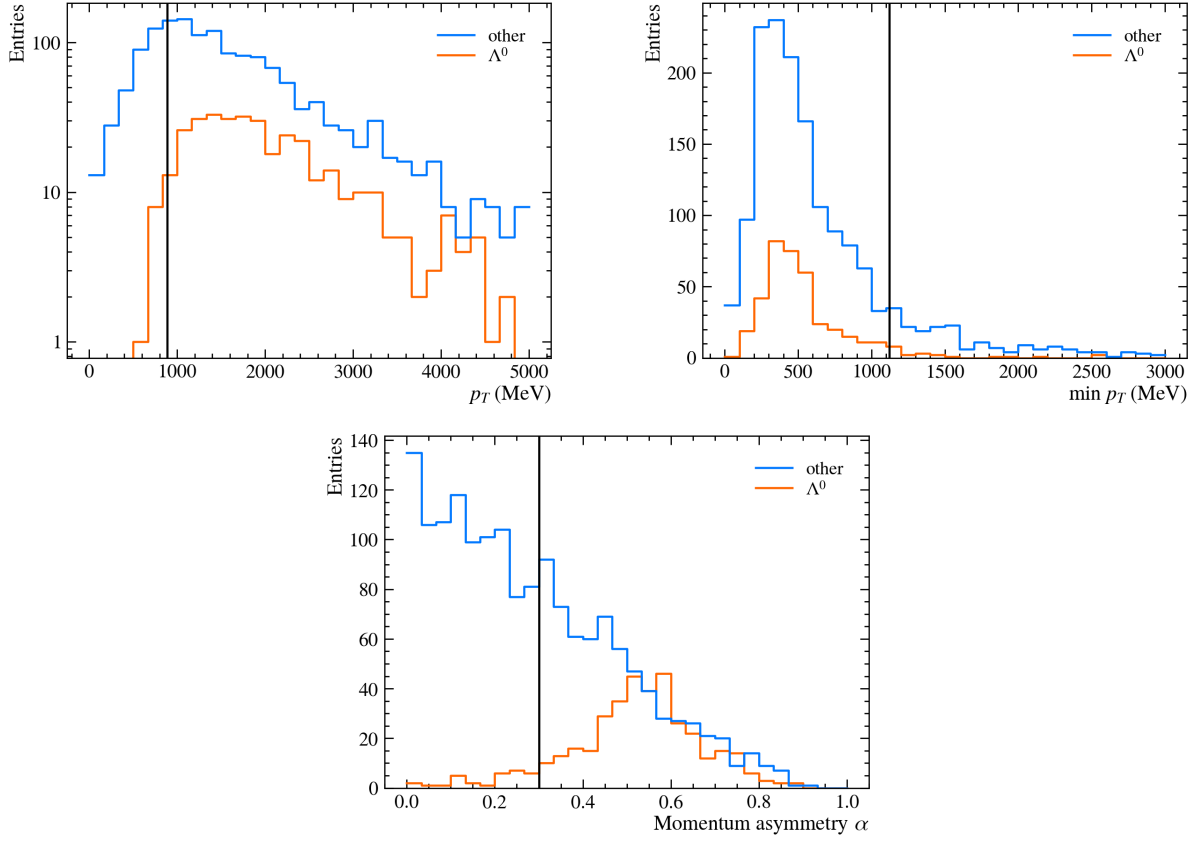


Figure 26: Distribution of selection variables for signal (Λ , orange) and background (everything else, blue) categories. The vertical black line represents the chosen cuts.

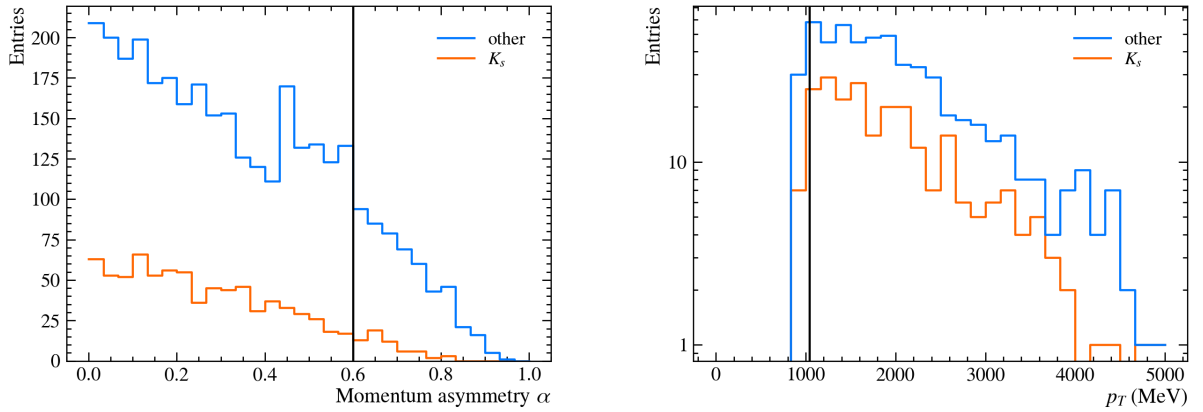


Figure 27: Distribution of selection variables for signal (K_S^0 , orange) and background (everything else, blue) categories. The vertical black line represents the chosen cuts.

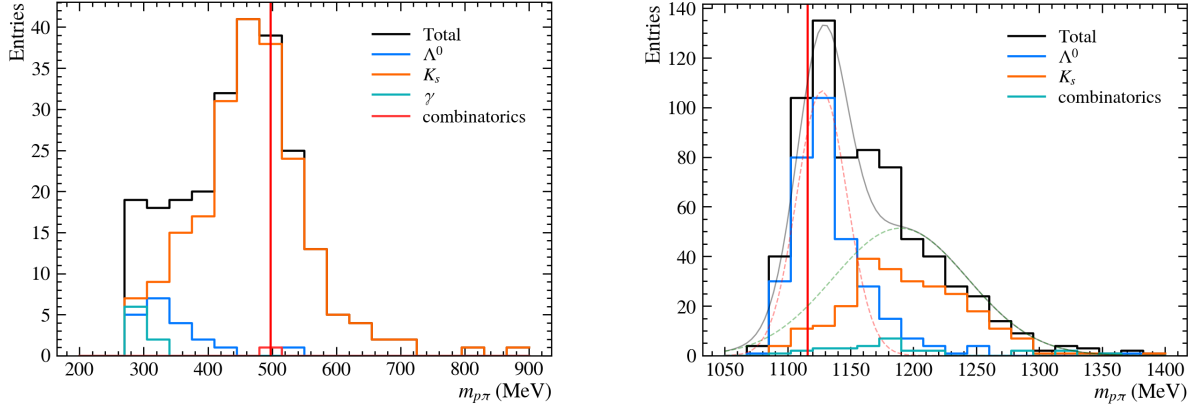


Figure 28: Mass distributions for K_S^0 (left) and Λ (right) particle candidates, that passed the selection cuts. The vertical red line represents the PDG value for the mass of each particle.

- Matching of the particles with ECAL and Muon clusters. Determination of Lepton ID⁶.
- *Faraway* vertex construction with two *faraway* particle candidates and their preselection.
- Fake track filtering and creation of composite particle candidates.
- Selection of composite particle candidates.

The sketch of the LHCb HLT1 execution sequence with the new *Faraway* algorithm is shown in Fig. 29. The HLT1 throughput drop from the inclusion of the *Faraway* recon-

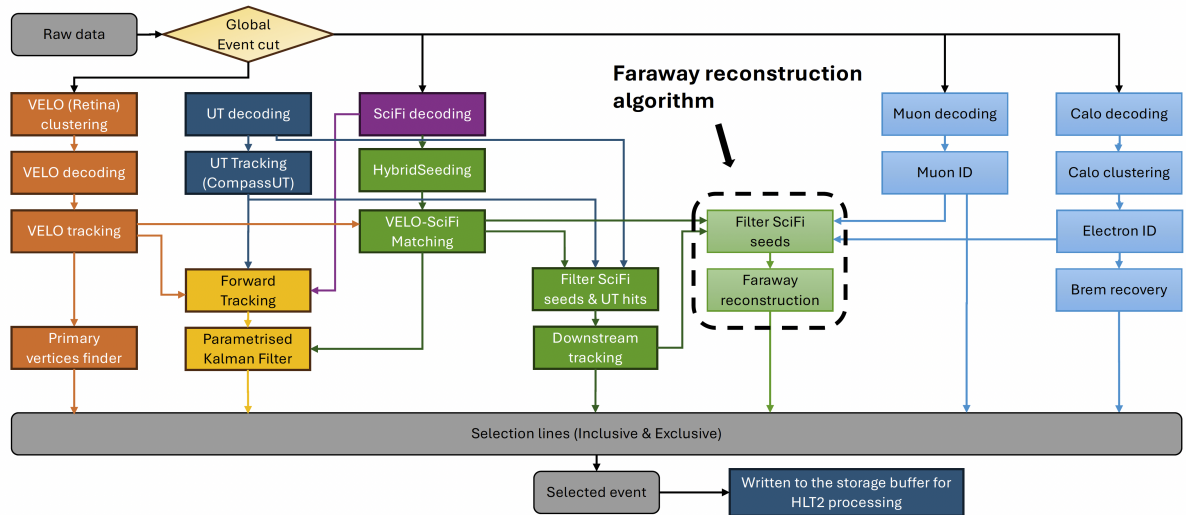


Figure 29: The LHCb HLT1 algorithm execution sequence. It includes decoding from raw data, reconstruction and selections. The algorithms that have been developed in the context of the current master thesis are highlighted with black dashed rectangle.

⁶Lepton ID contains information if the particle is likely to be an electron or muon. It is estimated using clusters in ECAL and hits in Muon stations.

struction algorithm is around 9% for NVIDIA RTX A5000 GPU (the one that is used during data-taking). Reference throughput (without **Faraway**) is 115.99 events/s while the throughput with **Faraway** is 104.94 events/s.

16 Algorithms performance

The mass histograms for K_S^0 and Λ particle candidates after all stages of **Faraway** reconstruction and selection, obtained using LHCb real data from April 20th *MEP*⁷ dump, are shown in Fig. 30. The distributions are fitted with a superposition of two Gauss probability density functions (pdfs) and a linear background.

The shift in the Λ plot may originate from a non-perfect trajectory function, which is obtained using the standard LHCb MC approach, as described in Sec. 11.3. As the magnetic field is non-homogeneous towards x and y axes, softer pions bend more towards the detector edge, while harder protons stay closer to the centre. This, together with the fact that the trajectory function is created using a Minimum Bias sample in which there are more particles closer to the centre and therefore they are better described, worsens the vertex reconstruction and biases the resulting mass plot. The possible ways to overcome this are described in the next section.

However, it is important to highlight that it is not crucial for physics performance to have a precise reconstruction at the HLT1 level since the whole event is reconstructed from scratch again at HLT2. But from another point of view, the unbiased distributions are very useful during the calibration process.

17 Prospects

There are different ways to proceed with the improvement of **Faraway** reconstruction algorithm. The first one is based on studies with particle gun, as described in Sec. 11.4, while the second one relies on external detectors in order to improve the reconstruction resolution.

17.1 Improvement of the trajectory function using MVA

The trajectory function dependence as a function of z is studied in section 11.4. However, it is possible to evaluate the dependence on other parameters using the particle gun approach, as it makes the extraction of exact trajectory function values straightforward. It can be done by assuming, that parameters in $f(z)$ dependency are not constants, but parameters of initial state \vec{s}_{SciFi} at the SciFi, which makes the trajectory function dependent on that as well $f(z, \vec{s}_{SciFi})$. In order to study these dependencies, the trajectory

⁷*MEP* dumps contain all the detector response and are performed before software triggers. They are mainly used for calibration and test purposes.

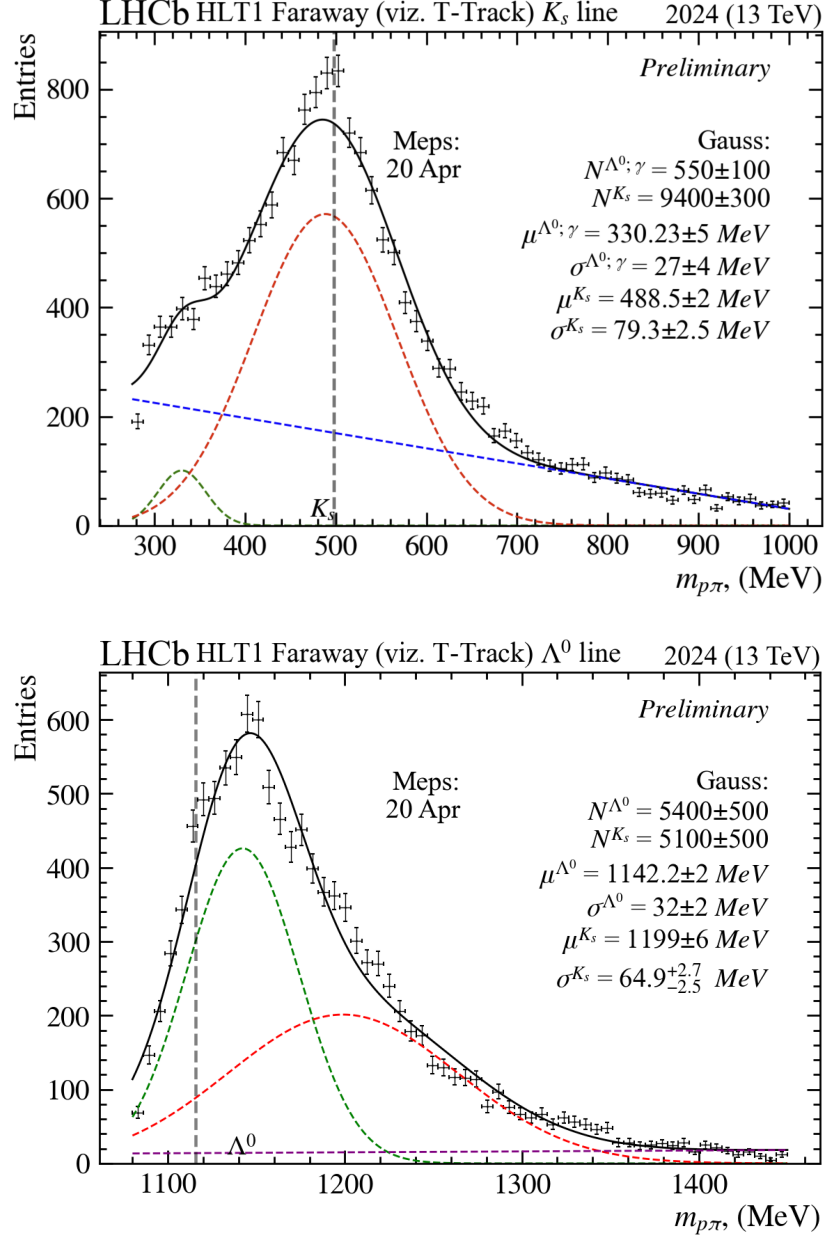


Figure 30: The mass distributions for K_S^0 (top) and Λ (bottom) particle candidates, obtained using LHCb real data from April, 20 *MEP* dump. The distributions are fitted with a superposition of two Gauss probability density functions (pdfs) and a linear background.

function of every particle is fitted assuming the parameters are free (Fig. 31), and then these parameters are plotted vs particle's initial state value (Fig. 32). The trajectory function model consists of 3 interpolation splines, linear function in the beginning (to satisfy condition $f(\bar{z})$ to be linear as $\bar{z} \rightarrow -\infty$) and exponential in the end:

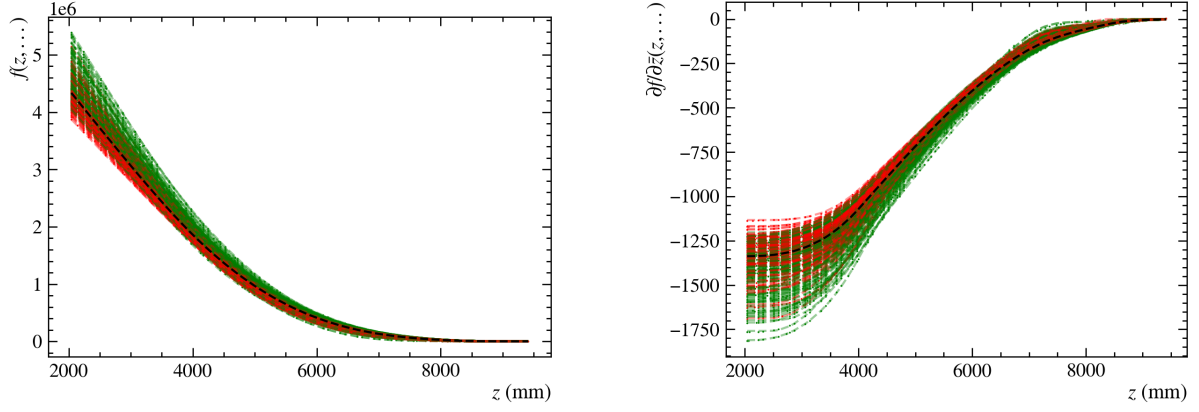


Figure 31: The fitted trajectory functions using model 17.1. The black line represents a curve with average parameters.

$$f'(z) = \begin{cases} a_1, & \text{if } \bar{z} \leq \bar{z}_{12} \\ y_2^A(1 - t_2) + t_2 y_2^B + t_2(1 - t_2)(a_2(1 - t_2) + t_2 b_2), & \text{if } \bar{z}_{12} < \bar{z} \leq \bar{z}_{23} \\ y_3^A(1 - t_3) + t_3 y_3^B + t_3(1 - t_3)(a_3(1 - t_3) + t_3 b_3), & \text{if } \bar{z}_{23} < \bar{z} \leq \bar{z}_{34} \\ y_4^A(1 - t_4) + t_4 y_4^B + t_4(1 - t_4)(a_4(1 - t_4) + t_4 b_4), & \text{if } \bar{z}_{34} < \bar{z} \leq \bar{z}_{45} \\ a_5 e^{b_5 \bar{z}} + c_5, & \text{otherwise} \end{cases} \quad (17.1)$$

where for $2 \leq i \leq 4$: $t_i = (\bar{z} - z_{i-1,i})/(z_{i,i+1} - z_{i-1,i})$, $y_i^{A,B}$, a_i , b_i - parameters of interpolation splines, some of which are chosen in a way that ensures continuity and smoothness of trajectory function. Parameters a_1 , a_5 , b_5 and c_5 are free. Other parameters are either free or fixed to a specific value, as shown in Table 1. At the time of writing the current thesis, the work on an evaluation of parameter dependence on the initial state at the SciFi (Fig. 32) is ongoing.

Parameter	Type	Value (if fixed)
a_1	free	
y_2^B	free	
b_2	free	
y_3^B	free	
b_3	free	
a_5	free	
b_5	free	
z_{12}	free	
z_{23}	fixed	-5410.0
z_{34}	fixed	-2410.0
z_{45}	fixed	-1000
c_5	fixed	0

Table 1: Summary of parameters, used in trajectory model 11.5.

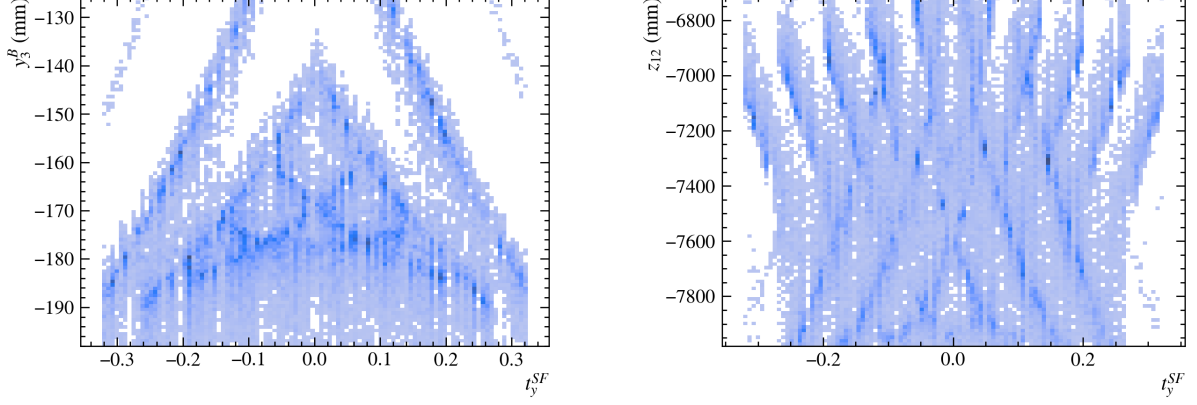


Figure 32: Dependence of the fitted parameters vs initial slope t_y at the SciFi. It is easy to see that there are correlations between the variables.

17.2 Usage of reconstruction information from other sub-detectors

One of the biggest challenges in *faraway* vertex reconstruction is the significant error in z_{outx} estimation (Fig. 23). It is clear that in order to find a vertex using $x - z$ plane, one has to have precise momentum measurements, which is not the case of *faraway* tracks (Fig. 18). On the other hand, due to the geometry of the SciFi subdetector (Sec. 6.3), the $y - z$ track resolution (Fig. 15) is not enough to be used alone in vertex reconstruction.

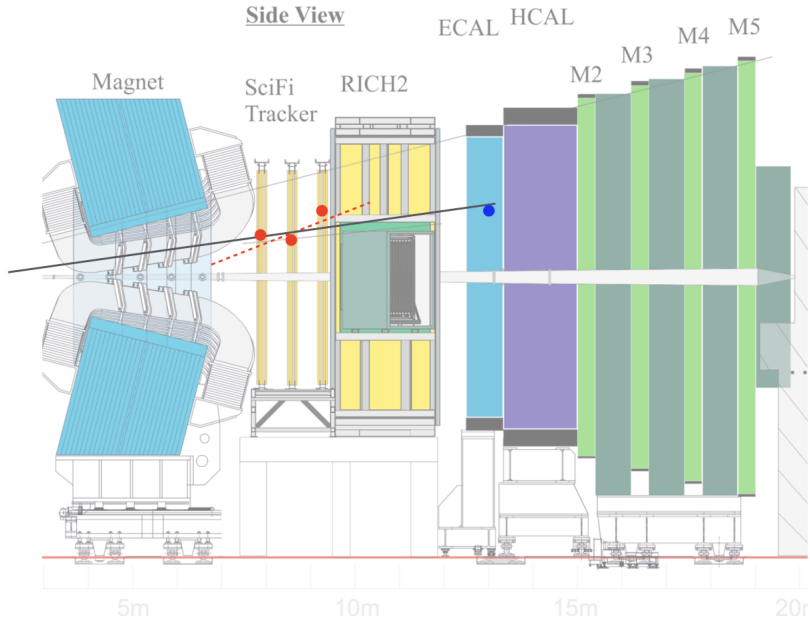


Figure 33: A sketch, demonstrating the usage of hit information from other subdetectors. The $y - z$ projection of the LHCb detector is shown as background. Red dots correspond to SciFi hits and the red dashed line represents the track candidate, reconstructed using these hits, as it is done currently. The blue dot is an ECAL cluster, that corresponds to the same particle and may be used for track reconstruction improvement (black line).

Therefore, it may be worth trying to exploit reconstructed information from other

subdetectors available at HLT1 and suitable for *faraway* tracks: ECAL, Muon chambers. The hits in these detectors may be associated with *faraway* track segments, and the y hit information may be used to improve track parameters (Fig. 33). The corresponding studies are at the initial stage at the time of writing this thesis.

17.3 The potential of *faraway* track reconstruction

It is important to highlight that the improvements to the **Faraway** reconstruction algorithm are crucial for future physics performance. Figure 34 shows the LHCb sensitivity

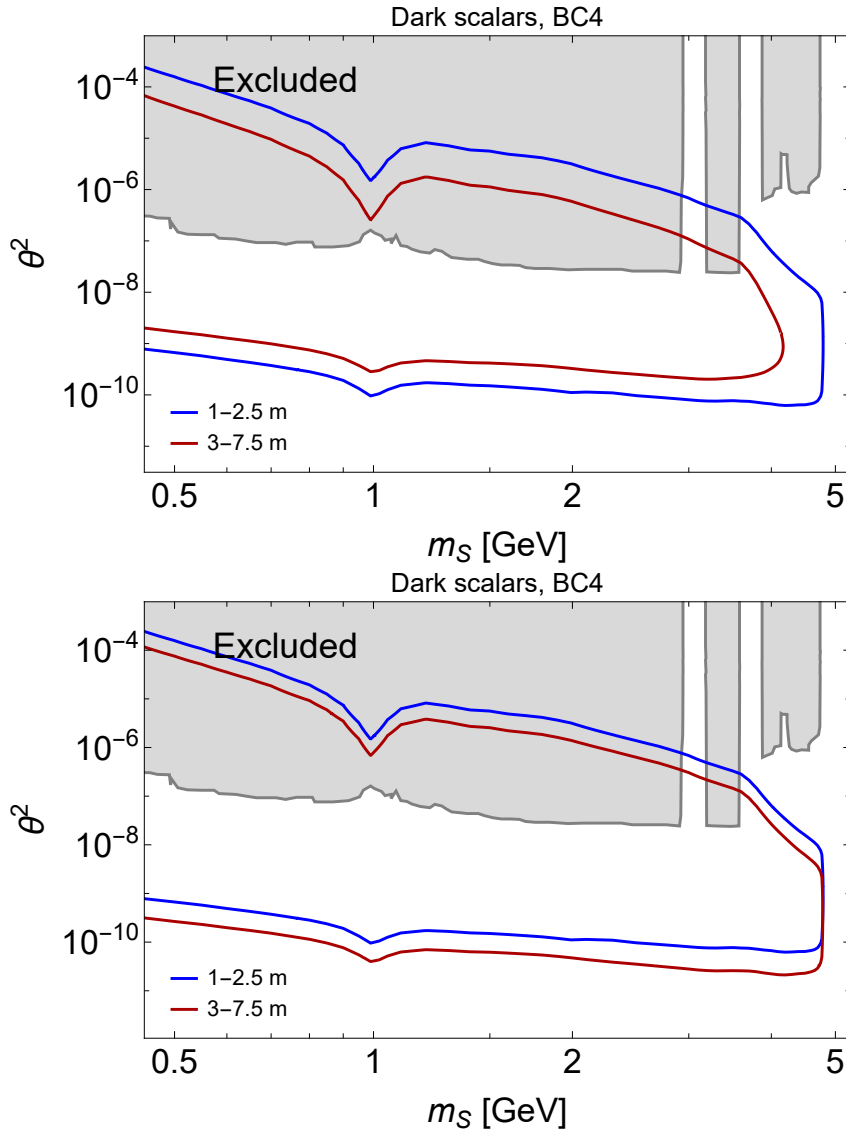


Figure 34: Sensitivity to Higgs-like scalars within model BC4. The blue line represents the LHCb sensitivity region with the **Downstream** reconstruction algorithm while the red one represents the sensitivity with **Faraway** algorithm with an assumption of the global efficiency of 1% (left) and 40% (right). The excluded parameter space (grey area) is taken from [40, 41, 42].

region obtained with the new **Faraway** reconstruction in two cases, with the global efficiency of 1% (closer to the current state) and 40%. The plots are obtained in the same

way as in Sec. 10. The left plot of Fig. 34 shows that due to low global efficiency, the sensitive region is completely covered by the **Downstream** reconstruction algorithm, while in the case of significant efficiency improvement, an extension can be achieved.

18 Conclusions.

This work presents the first implementation of the **Faraway** track reconstruction algorithm at the first High-Level Trigger of the LHCb experiment.

Extensive studies regarding the particle trajectory in the LHCb magnet region are conducted and corresponding strategies for a fast track parameterisation are developed. In addition, the methodology to measure track momentum is elaborated, with an achieved momentum resolution of 15%.

An algorithm for vertex reconstruction using *faraway* tracks is developed. It is based on the numerical minimisation of the smallest distance between two tracks (DOCA). The obtained resolution in the z coordinate for the vertex position is around 1 m. This large uncertainty may be the cause of a bias in the mass distribution for Λ particles, and in addition, be the origin of the reduced efficiency in the selection process.

The developed selection procedures efficiently remove the fake composite candidates thanks to the use of a fast and performant single-layer fully connected neural network. The fake composite contamination in the output of the algorithm is below 1%.

The **Faraway** reconstruction algorithm is already implemented in the LHCb HLT1 system. It may be improved in the coming months with the aim of its participation in the data-taking during 2025. The impact of this algorithm on the physics performance of LHCb is notable. Trigger efficiencies for decay channels involving b - and c -baryons are expected to increase. In addition, measurements of electric dipole moments (EDM) with strange hadrons can benefit from triggering *faraway* track candidates. On top of this, since the available decay volume for reconstruction can be significantly increased, this algorithm may play an important role in LHCb BSM searches for lifetimes ranging up to several nanoseconds. It may be the key to the new discoveries in the coming years.

References

- [1] A. Arbuzov, “Quantum field theory and the electroweak standard model,”.
- [2] A. Collaboration *et al.*, “Observation of a new particle in the search for the Standard Model Higgs boson with the ATLAS detector at the LHC,” *arXiv preprint arXiv:1207.7214* (2012) .
- [3] C. Collaboration *et al.*, “Observation of a new boson at a mass of 125 GeV with the CMS experiment at the LHC,” *arXiv preprint arXiv:1207.7235* (2012) .
- [4] M. E. Peskin, *An introduction to quantum field theory*. CRC press, 2018.
- [5] P. W. Higgs, “Broken symmetries and the masses of gauge bosons,” *Physical review letters* **13** no. 16, (1964) 508.
- [6] F. Englert and R. Brout, “Broken symmetry and the mass of gauge vector mesons,” *Physical review letters* **13** no. 9, (1964) 321.
- [7] B. K. Jashal, “Triggering new discoveries: development of advanced HLT1 algorithms for detection of long-lived particles at LHCb.” 2023.
<https://cds.cern.ch/record/2881886>. Presented 07 Nov 2023.
- [8] L. Lee, C. Ohm, A. Soffer, and T.-T. Yu, “Collider searches for long-lived particles beyond the Standard Model,” *Progress in Particle and Nuclear Physics* **106** (2019) 210–255.
- [9] R. Allahverdi, N. P. D. Loc, and J. K. Osiński, “Dark matter and baryogenesis from visible-sector long-lived particles,” *Physical Review D* **107** no. 12, (June, 2023) .
<http://dx.doi.org/10.1103/PhysRevD.107.123510>.
- [10] P. Barnes, Z. Johnson, A. Pierce, and B. Shakya, “Simple hidden sector dark matter,” *Physical Review D* **102** no. 7, (Oct., 2020) .
<http://dx.doi.org/10.1103/PhysRevD.102.075019>.
- [11] A. M. Abdullahi, P. Barham Alzás, *et al.*, “The present and future status of heavy neutral leptons,” *Journal of Physics G: Nuclear and Particle Physics* **50** no. 2, (Jan., 2023) 020501. <http://dx.doi.org/10.1088/1361-6471/ac98f9>.
- [12] S. M. Barr, “Solving the strong CP problem without the Peccei-Quinn symmetry,” *Physical Review Letters* **53** no. 4, (1984) 329.
- [13] R. Aaij, B. Adeva, *et al.*, “Search for massive long-lived particles decaying semileptonically in the LHCb detector,” *The European Physical Journal C* **77** (2017) 1–16.

- [14] R. Aaij, B. Adeva, *et al.*, “Updated search for long-lived particles decaying to jet pairs,” *The European Physical Journal C* **77** (2017) 1–14.
- [15] R. Aaij, B. Adeva, *et al.*, “Search for Higgs-like bosons decaying into long-lived exotic particles,” *The European Physical Journal C* **76** (2016) 1–15.
- [16] **LHCb** Collaboration, R. Aaij *et al.*, “Search for Majorana neutrinos in $B^- \rightarrow \pi^+ \mu^- \mu^-$ decays,” *Phys. Rev. Lett.* **112** no. 13, (2014) 131802, [arXiv:1401.5361 \[hep-ex\]](#).
- [17] R. Aaij, C. Abellan Beteta, *et al.*, “Searches for Majorana neutrinos in B-decays,” *Physical Review D—Particles, Fields, Gravitation, and Cosmology* **85** no. 11, (2012) 112004.
- [18] R. Aaij, B. Adeva, *et al.*, “Search for hidden-sector bosons in $B^0 \rightarrow K^{*0} \mu^+ \mu^-$ decays,” *Physical review letters* **115** no. 16, (2015) 161802.
- [19] **LHCb** Collaboration, R. Aaij *et al.*, “Search for long-lived scalar particles in $B^+ \rightarrow K^+ \chi(\mu^+ \mu^-)$ decays,” *Phys. Rev. D* **95** no. 7, (2017) 071101, [arXiv:1612.07818 \[hep-ex\]](#).
- [20] R. Aaij, B. Adeva, *et al.*, “Search for long-lived heavy charged particles using a ring imaging Cherenkov technique at LHCb,” *The European Physical Journal C* **75** (2015) 1–14.
- [21] **LHCb** Collaboration, R. Aaij *et al.*, “Search for $A' \rightarrow \mu^+ \mu^-$ Decays,” *Phys. Rev. Lett.* **124** no. 4, (2020) 041801, [arXiv:1910.06926 \[hep-ex\]](#).
- [22] J. Alimena *et al.*, “Searching for long-lived particles beyond the Standard Model at the Large Hadron Collider,” *J. Phys. G* **47** no. 9, (2020) 090501, [arXiv:1903.04497 \[hep-ex\]](#).
- [23] L. Henry, B. Jashal, V. Kholoimov, D. Mendoza, A. Oyanguren, V. Svintozelskyi, and J. Zhuo, “Impact of the high-level trigger for detecting long-lived particles at LHCb,” *EPJ Web Conf.* **295** (2024) 02015.
- [24] **LHCb** Collaboration, R. Aaij *et al.*, “The LHCb upgrade I,” [arXiv:2305.10515 \[hep-ex\]](#).
- [25] V. Gorkavenko, B. K. Jashal, V. Kholoimov, Y. Kyselov, D. Mendoza, M. Ovchinnikov, A. Oyanguren, V. Svintozelskyi, and J. Zhuo, “Lhcb potential to discover long-lived new physics particles with lifetimes above 100 ps,” *The European Physical Journal C* **84** no. 6, (June, 2024) .
<http://dx.doi.org/10.1140/epjc/s10052-024-12906-3>.

- [26] **LHCbcollaboration** Collaboration, I. Bediaga, J. M. De Miranda, *et al.*, “Framework TDR for the LHCb Upgrade: Technical Design Report,” tech. rep., 2012. <https://cds.cern.ch/record/1443882>.
- [27] T. L. Collaboration, A. A. A. Jr, *et al.*, “The lhcb detector at the lhcb,” *Journal of Instrumentation* **3** no. 08, (Aug, 2008) S08005. <https://dx.doi.org/10.1088/1748-0221/3/08/S08005>.
- [28] **LHCb** Collaboration, “LHCb Trigger and Online Upgrade Technical Design Report,”.
- [29] **LHCb** Collaboration, “LHCb Tracker Upgrade Technical Design Report,”.
- [30] L. collaboration, R. Aaij, *et al.*, “Long-lived particle reconstruction downstream of the lhcb magnet.” 2024. <https://arxiv.org/abs/2211.10920>.
- [31] **LHCb** Collaboration, “Dataflow diagrams for LHCb user analysis in Run 3 ,” . <https://cds.cern.ch/record/2896664>.
- [32] R. Aaij, S. Benson, *et al.*, “A comprehensive real-time analysis model at the LHCb experiment,” *Journal of Instrumentation* **14** no. 04, (2019) P04006–P04006.
- [33] R. Aaij, S. Amato, *et al.*, “Tesla: an application for real-time data analysis in High Energy Physics,” *Computer Physics Communications* **208** (2016) 35–42.
- [34] C. Fitzpatrick and V. V. Gligorov, “Anatomy of an upgrade event in the upgrade era, and implications for the LHCb trigger,”.
- [35] D. H. C. Pérez, N. Neufeld, and A. R. Núñez, “Search by triplet: An efficient local track reconstruction algorithm for parallel architectures,” *Journal of Computational Science* **54** (2021) 101422.
- [36] R. E. Kalman, “A new approach to linear filtering and prediction problems,”.
- [37] R. Aaij, J. Albrecht, *et al.*, “Allen: A high-level trigger on gpus for lhcb,” *Computing and Software for Big Science* **4** no. 1, (Apr., 2020) . <http://dx.doi.org/10.1007/s41781-020-00039-7>.
- [38] S. Aiola, Y. Amhis, *et al.*, “Hybrid seeding: A standalone track reconstruction algorithm for scintillating fibre tracker at LHCb,” *Computer Physics Communications* **260** (2021) 107713.
- [39] L. Calefice, “Standalone track reconstruction on GPUs in the first stage of the upgraded LHCb trigger system & Preparations for measurements with strange hadrons in Run 3.” 2022. <https://cds.cern.ch/record/2856339>. Presented 13 Dec 2022.

- [40] C. Antel, M. Battaglieri, *et al.*, “Feebly interacting particles: Fips 2022 workshop report.” 2023. <https://arxiv.org/abs/2305.01715>.
- [41] A. Boyarsky, M. Ovchinnikov, O. Ruchayskiy, and V. Syvolap, “Improved big bang nucleosynthesis constraints on heavy neutral leptons,” *Physical Review D* **104** no. 2, (July, 2021) . <http://dx.doi.org/10.1103/PhysRevD.104.023517>.
- [42] N. Sabti, A. Magalich, and A. Filimonova, “An extended analysis of heavy neutral leptons during big bang nucleosynthesis,” *Journal of Cosmology and Astroparticle Physics* **2020** no. 11, (Nov., 2020) 056–056.
<http://dx.doi.org/10.1088/1475-7516/2020/11/056>.
- [43] X.-S. Yang, “Chapter 20 - numerical methods,” in *Engineering Mathematics with Examples and Applications*, X.-S. Yang, ed., pp. 231–241. Academic Press, 2017.
<https://www.sciencedirect.com/science/article/pii/B9780128097304000276>.
- [44] S. Agostinelli, J. Allison, *et al.*, “Geant4—a simulation toolkit,” *Nuclear Instruments and Methods in Physics Research Section A: Accelerators, Spectrometers, Detectors and Associated Equipment* **506** no. 3, (2003) 250–303.
<https://www.sciencedirect.com/science/article/pii/S0168900203013688>.